Title
Identification of novel light-activated chemical tools for the study of TRPA1-mediated non-visual photosensation

Author
Cheng, Darya Cinyee

Publication Date
2020

Peer reviewed|Thesis/dissertation

Identification of novel light-activated chemical tools for the study of TRPA1-mediated non-visual photosensation

by
Darya Cinyee Cheng

DISSERTATION
Submitted in partial satisfaction of the requirements for degree of
DOCTOR OF PHILOSOPHY

in

Pharmaceutical Sciences and Pharmacogenomics

in the

GRADUATE DIVISION
of the
UNIVERSITY OF CALIFORNIA, SAN FRANCISCO

Approved:

DocuSigned by:
DAVID KOKEL
A6D68EDCBBD8452...

DAVID KOKEL
Chair

DocuSigned by:
Su Guo

Su Guo

DocuSigned by:
Jason Gestwicki
4909848DBB404E5...

Jason Gestwicki

Committee Members

ACKNOWLEDGMENTS

The work presented in this dissertation would not have been possible without the support and guidance of many people. Without their help, I would not have been able to overcome the many challenges and obstacles I faced over the past six years in order to successfully complete my research and write this dissertation.

I would like to thank the current and former members of my lab, without whom my research would not have been possible. I would first like to thank my advisor, Dr. Dave Kokel, for the opportunity to conduct research in his lab and for providing the tools and resources that allowed me to successfully complete this journey. Thank you also to Matt McCarroll, who, in addition to serving as a great source of knowledge, support, and feedback, went above and beyond to keep our research running smoothly. To Jack Taylor, thank you for all your help with my experiments, but thank you even more for your positivity and humor that made even the most difficult days more enjoyable. I also want to thank Douglas Myers-Turnbull, Cole Helsell, and Chris Ki, not only for all your efforts in designing and constructing our software and experimental tools, but also for your patience and advice as I learned to use them. To my fellow PSPG students Reid Kinser and Tia Tummino, thank you for all of your support and feedback. It has been a difficult journey for us all, and I can only hope that I was able to provide as much support and encouragement to everyone in the lab as you each did for me.

I would also like to thank Dr. Lennart Mucke and the members of his lab. Though I was not there long, I learned quite a lot about conducting excellent scientific research during that time. Beyond science, I also learned to trust in my ability to succeed, and not to let others derail me from my goals. In particular, I would like to thank Mark Evans for his patient guidance and mentorship of an untrained, first-year graduate student. With your help I quickly gained a great deal of

experience that has stayed with me throughout my time in graduate school, and your friendship made my experience in the lab much better than it otherwise would have been.

Many other mentors have helped me navigate graduate school and contributed to my development as a scientist. First, I would like to thank my thesis committee members. I want to thank Dr. Jason Gestwicki, who has been a major source of positivity and support. I cannot thank you enough for your scientific feedback and suggestions, and your advice has been invaluable when handling tough situations. To Dr. Su Guo, thank you for your input as part of my thesis committee. Even before that, however, your mentorship when I was a first-year student rotating in your lab was deeply appreciated, and I truly enjoyed my time there. Additionally, I would like to thank Dr. Deanna Kroetz, the previous PSPG program director, and Rebecca Dawson, the PSPG program administrator, for their support. From labs to funding to emotional support, I can say with certainty that without your help I would not have completed my degree.

Finally, I would like to thank my friends and family. Fellow PSPG graduate students, thank you for being such great friends. Whether it was commiserating over stalled projects, or going out for dinner, or giving feedback on a talk, I am so glad that you have been there for me. To my family – Mom, Dad, and Deric – thank you so much for your ongoing support and love. They have kept me going even when I doubted myself. To my parents especially, the values, skills, and love of learning you instilled in me have helped me to succeed. Though I may have rolled my eyes as a teenager, I see now how often you were right, and the things you taught me have served me well. Finally, to my partner, Jordan: thank you for having been there for me every step of the way. You've shared in my frustrations and my successes, my sadness and my joy, and my fears and excitement; you made adversity bearable and every step forward an achievement to be celebrated. You truly know me for who I am, and I could not ask for more.

CONTRIBUTIONS

Chapter 2 was modified from a manuscript in preparation titled “Identification of compounds producing non-visual photosensation via TrpA1 in zebrafish”. Darya C. Cheng contributed to study design and analysis. Darya C. Cheng, Matthew N. McCarroll, Jack C. Taylor, and Taia Wu contributed to experimental execution. Darya C. Cheng wrote the manuscript with contributions from David Kokel.

Identification of novel light-activated chemical tools

for the study of TRPA1-mediated non-visual photosensation

Darya Cinyee Cheng

ABSTRACT

Over the past decade, the transient receptor potential ankyrin 1 (TRPA1) receptor has been extensively studied because of its wide distribution across the human body and its roles in many aspects of sensation, some of which are physiological and others of which are pathophysiological. A member of the TRP channel family, TRPA1 is most commonly found in somatosensory neurons present in nociceptors, especially the dorsal root ganglia and trigeminal ganglia, but its expression has been reported in tissues as disparate as the cells of the inner ear, non-neuronal cells in the small and large intestines and lungs, and in the beta islet cells of the pancreas. Physiologically, TRPA1's primary role is as a nociceptive chemosensor detecting exogenous agonists that are irritants, such as AITC from wasabi, and endogenous agonists that are indicators of oxidative stress, such as H_2O_2. However, when TRPA1 becomes dysregulated, its physiological roles can become distorted. Research has demonstrated that TRPA1 is involved in many pathologies including chronic pain and inflammation, neuropathic pain, itch, and respiratory diseases, but to date, few TRPA1-targeting therapeutics have been successful, and it is evident that greater understanding of the receptor is required to address this need. Recently, the discovery of optovin revealed that a synthetic photoreactive compound could confer photosensitivity onto vertebrate TRPA1, but much is still unknown about photo-dependent TRPA1 activation. One way to approach this question is through identification of additional chemotypes that act similarly to optovin. In this dissertation, I describe the process of identifying such compounds and the characterization of their properties. Analysis of data from a large-scale, behavior-based chemical screen conducted in larval zebrafish established a small

subset of compounds that induced a strong behavioral response to light. Structural analysis showed that the hit compounds were in fact structurally diverse, and photochemical, behavioral, and toxicity studies uncovered characteristics unique to each compound. Experiments using TRPA1 mutant zebrafish confirmed that a subset of these hits are TRPA1-dependent. Together, these structurally, photochemically, and pharmacologically diverse compounds form a tool set that can be used to modulate the TRPA1 receptor, allowing future researchers to gain a better understanding of the receptor's characteristics and mechanisms, research its roles in sensation and photo-behaviors, and identify therapeutics to address pathologies caused by its dysregulation.

TABLE OF CONTENTS

LIST OF FIGURES

LIST OF TABLES

Chapter 1: The TRPA1 receptor as a research and therapeutic target

The transient receptor potential ankyrin 1, or TRPA1, receptor is one of 28 members of the transient receptor potential (TRP) channel family. Structurally, it comprises four identical subunits, each of which contains six transmembrane alpha helices. These subunits surround a central pore and selectivity filter, which is formed from the fifth and sixth helices of each subunit[1]. The intracellular N-terminal domain contains the "allosteric nexus", which contains the binding site for many agonists[2], along with 14-18 ankyrin repeats depending on the species[1] (**Fig. 1.1**). TRPA1 is found most commonly in somatosensory neurons present in nociceptors, such as the dorsal root ganglia and trigeminal ganglia, but has also been reported in cell types as varied as the hair cells of the inner ear, non-neuronal epithelial cells in the small and large intestine, non-neuronal lung cells (including fibroblasts and smooth muscle cells), and in the insulin-producing beta islet cells of the pancreas. Once an agonist binds, TRPA1 becomes permeable to cations such as Na^+ and Ca^{2+}, which depolarize the membrane and initiate Ca^{2+} signaling in the cell.[1] (**Fig. 1.2**).

Physiological roles of the TRPA1 receptor

TRPA1 shares loose identity with the TRPV1 channel, which is responsible for the "hot" sensation caused by capsaicin in hot peppers[3]. Similarly, TRPA1 is responsible for the burning, "sinus-clearing" sensation that is induced when consuming foods such as wasabi or cinnamon, which contain allyl isothiocyanate (AITC)[4] and cinnamaldehyde (CA)[1], respectively. These exogenous electrophilic agonists, along with other compounds such as acrolein (from diesel exhaust) and allicin (from garlic extract), form covalent adducts with reactive cysteine and lysine residues in the allosteric nexus (**Fig. 1.1**). Together, these observations suggest that one of TRPA1's major roles is as a nociceptive chemosensor that induces pain when activated (**Fig. 1.2**), thereby serving as a warning to limit further exposure to the reactive irritant[1].

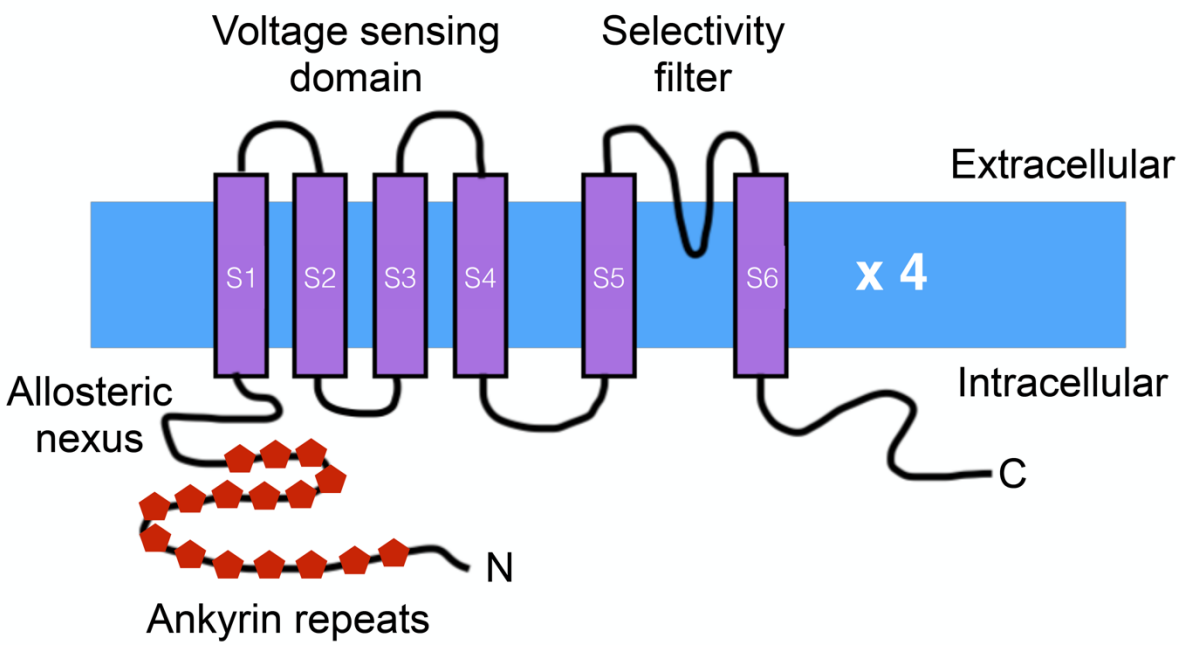

Figure 1.1 TRPA1 channel structure
TRPA1 is homotetramer, comprising four identical subunits, one of which is depicted here. Each subunit contains six transmembrane alpha helices (labeled S1-S6). In the N-terminal domain, the allosteric nexus (with reactive cysteine and lysine residues) can be found, along with the 14-18 ankyrin repeats that give TRPA1 its name. Together, the four subunits surround a central pore with a selectivity filter formed from the region between helices S5 and S6. (Adapted from Chen and Hackos 2015[1]).

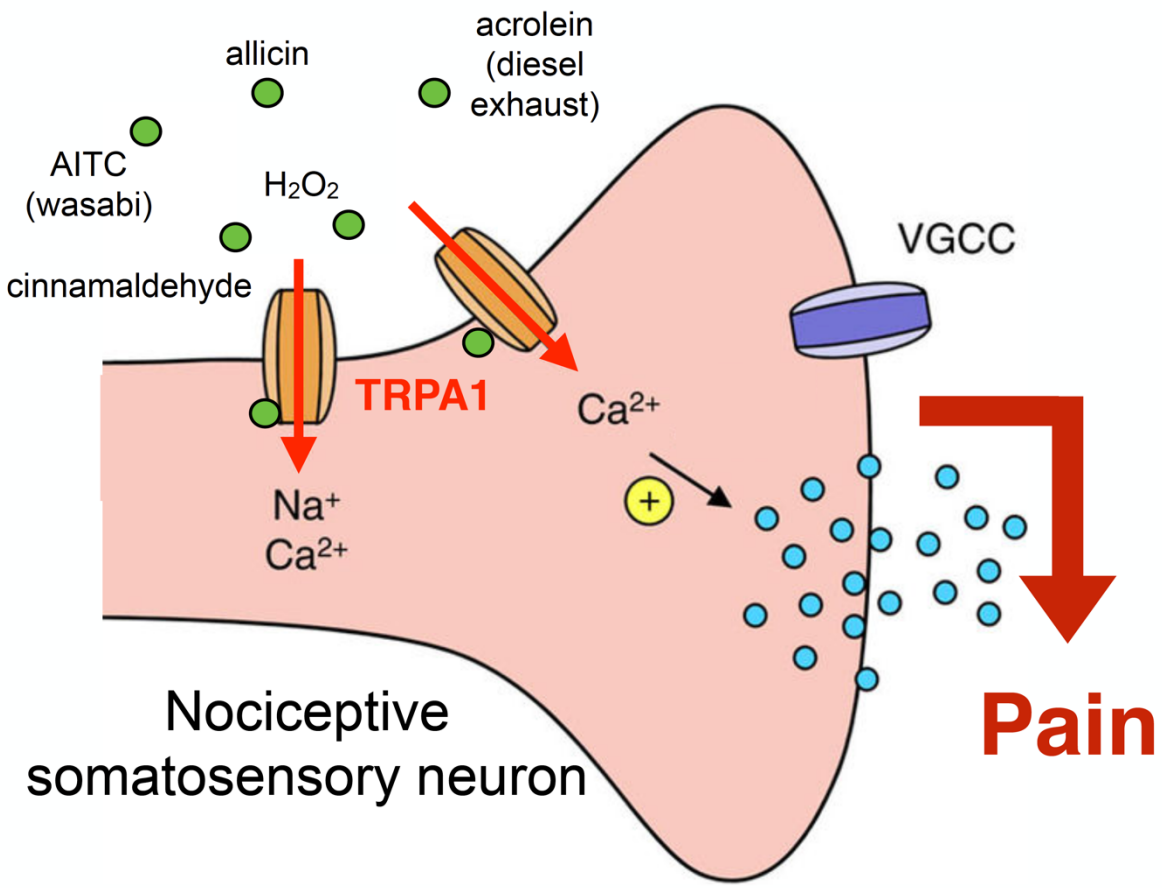

Figure 1.2 TRPA1 is found on nocicpetive somatosensory neurons
Following TRPA1 activation by either exogenous agonists (such as AITC, cinnamaldehyde, acrolein, and allicin) or endogenous agonists (such as H_2O_2), TRPA1 becomes permeable to cations such as Na^+ and Ca^{2+}, which depolarize the membrane and initiate Ca^{2+} and neurotransmitter signaling. Because TRPA1 channels are most commonly expressed in the somatosensory neurons of nociceptors, activation of TRPA1 can result in the sensation of pain. (Adapted from Andersson et al. 2011[5]).

Additionally, TRPA1 can also be activated endogenously. Agonists include oxidized lipids, nitrated lipids, and reactive oxygen species (ROS) such as H_2O_2[6], all of which may act as indicators of oxidative stress[1]. Likewise, TRPA1 can be activated as part of the downstream pathway of G-protein coupled receptors. One such pathway is through the phospholipase-C coupled receptors that detect pruritic and pro-inflammatory agents, thus forming a direct link between TRPA1 and the sensation of itch[2]. Finally, TRPA1 has also been implicated in other modes of nociception, including mechanosensitivity[7], heat sensitivity[8], and cold sensitivity[9].

Pathophysiological roles of TRPA1

Though TRPA1 plays an important role in nociception, its dysregulation has been implicated in several pathophysiologies, many of which are distorted versions of TRPA1's normal functions. Most notably, TRPA1 has been shown to play a major role in pain and inflammation. A gain-of-function mutation in TRPA1 causes a genetic disorder known as familial episodic pain syndrome that is characterized by debilitating upper body pain[10]. Likewise, TRPA1 has been demonstrated to play a role in neuropathic pain, a form of pain which is due to nervous system damage or dysfunction rather than tissue injury[11]. Increased expression of TRPA1 receptors has been reported at sites of nerve injury[12], and methylglyoxal, a reactive compound produced in large amounts in diabetes, activates TRPA1[13], while TRPA1 blockade reduces hypersensitivity arising from diabetic neuropathy[14]. Chemotherapy-induced peripheral neuropathy is likewise thought to be mediated through TRPA1, potentially through oxidative stress by-products produced following exposure to chemotherapy drugs[11,15]. Chronic inflammation has been linked to TRPA1 as well. While acute inflammation is important and useful in signaling the immune system to repair damage and heal the body, chronic inflammation and pain is detrimental, and studies have shown that many of the proinflammatory agents released as part of the "inflammatory soup", such as ROS and oxidized or nitrated lipids[4], are TRPA1 activators[11].

In addition to pain and inflammation, TRPA1 is also known to be involved in other pathologies. Beyond its role in physiological levels of pruritus, elevated expression levels have been observed in atopic dermatitis lesions in both humans and mice[16], while TRPA1 antagonists were able to attenuate itch-scratching behaviors in mouse models of allergic contact dermatitis[17]. Chronic activation of TRPA1 has also been observed in respiratory diseases. Due to its function as a chemosensor, including as a sensor of airborne irritants, TRPA1 is highly expressed in the lungs and airways[1]. In conditions such as chronic cough, rhinitis, asthma, and chronic obstructive pulmonary disease (COPD), TRPA1 expression levels are elevated, and activation of receptors in these regions is greatly increased by elevated levels of both endogenous TRPA1 ligands and pro-inflammatory mediators[1].

By virtue of its involvement in these and other pathophysiologies, many of which have few or no treatments, TRPA1 represents a promising therapeutic target. Novel chronic pain medications targeting TRPA1 may help relieve neuropathic pain, while alternatives to common pain relievers with unwanted side effects, like acetaminophen (hepatotoxicity)[18] and ibuprofen (adverse gastrointestinal effects)[19] - both of which are thought to act at least partially through TRPA1[1,20] - might be developed. Likewise, as evidence has shown that antagonists and blockade of the TRPA1 receptors can attenuate the effects of many conditions, including airway pathologies and itch, novel antagonists could also address the unmet need for therapeutics in these areas.

Optovin: a reversible, light-activated TRPA1 agonist

Recently, the discovery of optovin revealed that pharmacological activation of TRPA1 can be modulated by light. Using 3dpf (days post fertilization) larval zebrafish, which are blind and do not respond to light, a large-scale behavior-based chemical screen of a 10,000 compound library was performed to search for hits that would allow for *in vivo*, optical control of endogenous channels[21]. This screen identified optovin (**Fig. 1.3**) as a compound that reliably

induced a strong period of motor activity following light exposure. Optovin-treated animals responded to stimulation by 387-nm (violet) light but not to other wavelengths, and multiple responses could be triggered with repeated pulses of light, showing that this novel, behavior-modifying compound could induce rapid and reversible motor excitation in response to violet light stimuli[21]. To determine whether the purple-light response behavioral profile was unique to optovin, the profiles for optovin and 700 known, annotated neuroactive compounds (including, but not limited to, compounds targeting the adrenergic, serotonergic, and glutamatergic pathways) were hierarchically clustered. Clustering revealed that the behavioral profile induced by optovin was unique, and that optovin was in fact on its own branch of the dendrogram (**Fig. 1.3**), suggesting that this compound is functionally distinct from known neuroactive compounds[21]. Further experiments identified TRPA1 as the receptor target for optovin. While wild type and heterozygous fish responded to violet stimuli, TRPA1 mutant fish did not. Transfection of HEK293T cells with human TRPA1 likewise demonstrated a response, as measured by calcium imaging, while green fluorescent protein (GFP) transfected cells did not[21]. Together, these results established that TRPA1 was both necessary and sufficient for the optovin response. As only a small subset of light-responsive TRPA1 receptors had been identified prior to optovin, this result represented a novel discovery that allowed for fine-tuned, spatiotemporal control of TRPA1 signaling via light in wild-type animals[21].

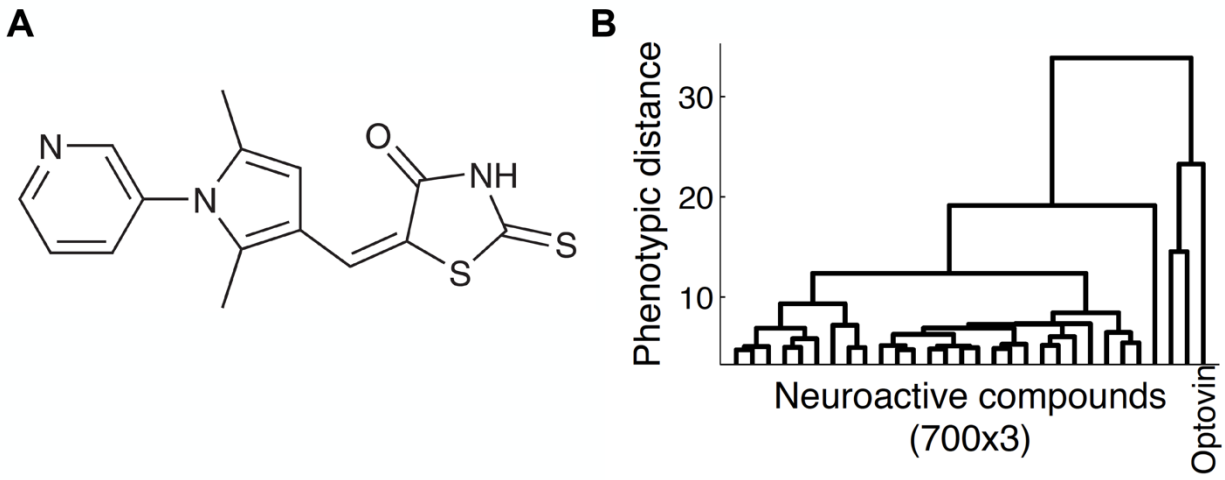

Figure 1.3 Optovin is functionally distinct from other known neuroactive compounds
A) The chemical structure of optovin[21]
B) Hierarchical clustering of optovin with 700 other known neuroactive compounds revealed that the behavioral profile produced by optovin is unique. Additionally, this demonstrates that behavioral phenotypes can be used to identify new compounds and classify known compounds, and that behavioral profiling can identify compounds with different mechanisms of action[21].

The need for novel light-dependent TRPA1 ligands

Though the discovery of optovin represents an exciting new direction for TRPA1 research, much is still unknown about light-dependent TRPA1 activation. One way to approach this question is through identification of additional chemotypes that act similarly to optovin. Though structural analysis has suggested that optovin's rhodanine ring may play an important role in its bioactivity, and several active structural analogues have been identified[22], it is still unclear exactly how the light activation of optovin occurs. Therefore, it would be interesting to compare it to other structures that have a light-dependent effect. Furthermore, while optovin itself is already a useful research tool that allows for real-time, optical control of TRPA1 and the cells in which it is expressed, novel compounds may possess properties that render them more suitable for different experimental purposes. For example, compounds may vary in their selectivity or specificity, target specific populations of TRPA1 receptors in different locations or tissues, induce unique patterns of response with varying levels of control, and/or demonstrate diversity in other properties such as potency, sustained effects, and toxicity. Together, these proposed tools could reveal previously unknown characteristics of the receptor and its roles, as well as contributing more broadly to the understanding of TRPA1-dependent or other non-visual photo-behaviors and light sensation in general in humans and other species. Finally, the discovery of more optovin-like compounds has the potential to lead to new therapeutics. As mentioned above, TRPA1 plays roles in pain, inflammation, and other pathophysiologies, so tools that target this receptor could be a starting point for new treatments. This goal is particularly important because current remedies for chronic pain, neuropathy, and other TRPA1-related conditions are often insufficient[22]. Such molecules could include new antagonists to block TRPA1's effects, but they could also include those with new mechanisms, such as agonists of TRPA1 subpopulations, which might achieve an analgesic effect, as with acetaminophen[5]. In this dissertation, I report on efforts to identify new chemical probes of TRPA1 using large-scale

zebrafish behavioral assays. The results of these studies provide important new chemotypes of manipulating TRPA1 and light-dependent behavior.

Large-scale screening to identify novel light-dependent TRPA1 ligands

In order to identify novel light-dependent TRPA1 ligands, we performed a large-scale, behavior-based novel chemical screen using larval zebrafish. While most high-throughput chemical screens are usually target based and performed *in vitro*, these methods have certain disadvantages; namely, they do not capture the full complexity of a vertebrate nervous system, and they make *a priori* assumptions about the targets of interest, thereby limiting their ability to detect compounds that achieve their effects through new pathways[23]. Given these limitations, we instead developed a system that screens compounds based on the behavioral phenotypes they induce in larval zebrafish in response to various stimuli. This method has a number of advantages over previous screening methods: first, by using zebrafish, we are able to capture behaviors from vertebrates with complex brains and nervous systems. As zebrafish and humans also share many conserved genes and neurotransmitter pathways, this provides results that are more relevant to humans than, for example, an isolated group of cells or *Drosophila*. Secondly, this method allows us to ascertain whether a compound has an effect *in vivo* during the early stages of screening before performing follow-up experiments. Finally, zebrafish larvae are small, relatively low cost, and they mature and reproduce quickly, making them suitable for high-throughput testing in a 96-well plate format, unlike mice or rats[23–25].

To perform these experiments, zebrafish embryos are first collected at 7dpf. Following the sorting of healthy and unhealthy animals, eight larvae are pipetted, along with egg water, into each well of a 96-well plate. The larvae are then treated with the compounds of interest, along with both positive and negative controls. The entire plate is then placed into our automated behavioral phenotyping instrument. Designed in-house, this instrument consists of a large box

containing a camera, lighting, and multiple apparatus for creating stimuli, including LEDs with varying wavelengths of light, solenoids to create physical “tapping” stimuli, and speakers for audio stimuli (**Fig. 1.4**). Once the instrument is closed to block off outside stimuli, a custom script runs to control the activation of predetermined groups of stimuli (“assays”) arranged into a series (a “battery”) (**Fig. 1.5**). Beyond the standardized screening battery, assays and batteries can also be adjusted and customized to probe different aspects of a behavioral phenotype. As the battery is run, the camera records the responses of the treated larvae. The resulting video footage is then converted into a series of motion index (MI) values (**Fig. 1.5**), which represent the change in pixels from one frame to the next as a measure of movement, where a higher MI value signifies increased activity, and a lower MI signifies decreased activity. The entire series of MI values is then plotted as a line graph, or MI trace, over time, along with a graphical indicator of the corresponding stimuli (**Fig. 1.5**). By analyzing these MI values and traces, we can identify patterns of behaviors that act as a “barcode” for specific mechanisms of action[24,25], and use that barcode to identify other compounds with similar phenotypes and mechanisms of action[26]. For example, one identified activity barcode is the “enhanced acoustic startle” response, characterized by a brief burst of activity in response to only one specific type of low-volume acoustic stimulus. This behavioral pattern was shown to be a signifier for $GABA_AR$ ligands[27]. The optovin response, in contrast, is a sharp but more sustained increase in activity in response to a violet light stimulus (**Fig. 1.5**).

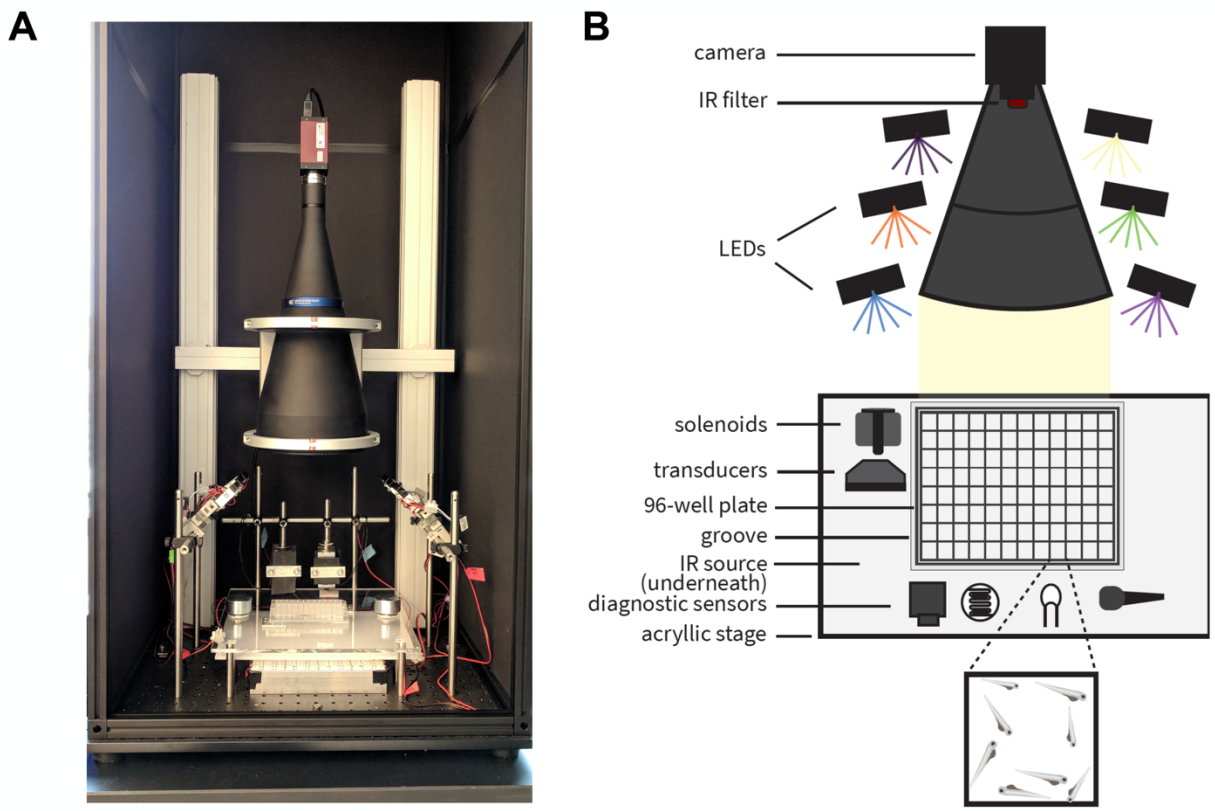

Figure 1.4 Automated behavioral phenotyping instrument
A) Photograph of the instrument
B) Schematic depicting instrument components. These include a camera, an infrared light source and visible-light blocking IR filter (to prevent confounding of the video images from stimuli light sources), an acrylic stage fitted with a groove to hold a 96-well plate, and diagnostic sensors. Stimuli apparatus include LEDs at various wavelengths, solenoids to produce a physical tap, and transducers to play audio[28].

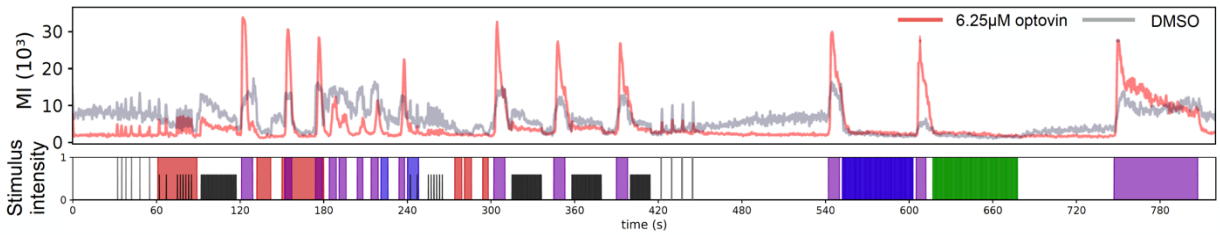

Figure 1.5 The optovin MI trace reveals that optovin induces a distinctive, violet light-dependent response

The motion index (MI, y-axis) is a measure of activity derived from the change in pixels from one frame of video to the next. The more pixels that have changed, the higher the MI, and the greater the activity. Here, the optovin (red) and DMSO (gray) MI values over time (x-axis) have been plotted together as MI traces for comparison. Along the bottom, a graphical depiction of stimuli at the time they occur allows for correlation to activity patterns. Blocks of color represent a light stimulus of the corresponding color. Vertical lines represent taps, with full lines representing a hard tap and the half lines representing a soft tap. The black rectangles are taps that occurred too closely together to be depicted separately. Optovin induces a distinct behavioral phenotype in which a sharp spike of activity occurs when the treated zebrafish larvae are exposed to violet light. Conversely, while there is a slight increase in activity in the DMSO-treated larvae, the response is no more than 50% that of the optovin-treated fish, and it does not form peaks.

Focus of the dissertation

The research described in this dissertation focuses on the discovery and characterization of novel, light-dependent, optovin-like compounds. The aim of this study is to identify these compounds and to furthermore confirm the optovin-like response as an indicator of light-dependent TRPA1 ligands. Using this behavioral phenotyping methodology, we screened a chemical library containing over 30,000 novel compounds. Manual and computational analyses of the MI traces revealed potential hits, and confirmatory experiments identified a set of hit compounds that induced behaviors similar to that of optovin. Photochemical, behavioral, and toxicity studies characterized the compounds and illustrated similarities and differences, while experiments with mutant TRPA1 fish confirmed that a subset of the hit compounds were in fact TRPA1 dependent. Overall, the findings from the work described herein contribute new insights into the light-dependent activation of TRPA1 as well as a set of novel prototype compounds with varying characteristics that control TRPA1 with light. Together, this will enable future researchers to not only further explore the physiological roles of TRPA1, but to better understand its pathophysiological roles and to develop therapeutics to address the unmet need in those areas.

REFERENCES

1. Chen, J. & Hackos, D. H. TRPA1 as a drug target—promise and challenges. *Naunyn-Schmiedeberg's Archives of Pharmacology* vol. 388 451–463 (2015).
2. Lin King, J. V. *et al.* A Cell-Penetrating Scorpion Toxin Enables Mode-Specific Modulation of TRPA1 and Pain. *Cell* **178**, 1362–1374.e16 (2019).
3. Rosenbaum, T. & Simon, S. A. TRPV1 Receptors and Signal Transduction. in *TRP Ion Channel Function in Sensory Transduction and Cellular Signaling Cascades* (eds. Liedtke, W. B. & Heller, S.) (CRC Press/Taylor & Francis, 2011).
4. Bautista, D. M., Pellegrino, M. & Tsunozaki, M. TRPA1: A gatekeeper for inflammation. *Annu. Rev. Physiol.* **75**, 181–200 (2013).
5. Andersson, D. A. *et al.* TRPA1 mediates spinal antinociception induced by acetaminophen and the cannabinoid Δ9-tetrahydrocannabiorcol. *Nat. Commun.* **2**, 551 (2011).
6. Alavi, M. S., Shamsizadeh, A., Karimi, G. & Roohbakhsh, A. Transient receptor potential ankyrin 1 (TRPA1)-mediated toxicity: friend or foe? *Toxicol. Mech. Methods* **30**, 1–18 (2020).
7. Brierley, S. M. *et al.* TRPA1 contributes to specific mechanically activated currents and sensory neuron mechanical hypersensitivity. *J. Physiol.* **589**, 3575–3593 (2011).
8. Cordero-Morales, J. F., Gracheva, E. O. & Julius, D. Cytoplasmic Ankyrin Repeats of Transient Receptor Potential A1 (TRPA1) Dictate Sensitivity to Thermal and Chemical Stimuli. *Biophysical Journal* vol. 102 23a (2012).
9. Sinica, V. *et al.* Human and Mouse TRPA1 Are Heat and Cold Sensors Differentially Tuned by Voltage. *Cells* **9**, (2019).
10. Kremeyer, B. *et al.* A gain-of-function mutation in TRPA1 causes familial episodic pain syndrome. *Neuron* **66**, 671–680 (2010).
11. Nassini, R., Materazzi, S., Benemei, S. & Geppetti, P. The TRPA1 Channel in Inflammatory

and Neuropathic Pain and Migraine. in *Reviews of Physiology, Biochemistry and Pharmacology, Vol. 167* (eds. Nilius, B. et al.) 1–43 (Springer International Publishing, 2014).

12. Anand, U. *et al.* TRPA1 receptor localisation in the human peripheral nervous system and functional studies in cultured human and rat sensory neurons. *Neurosci. Lett.* **438**, 221–227 (2008).
13. Andersson, D. A. *et al.* Methylglyoxal evokes pain by stimulating TRPA1. *PLoS One* **8**, e77986 (2013).
14. Wei, H., Hämäläinen, M. M., Saarnilehto, M., Koivisto, A. & Pertovaara, A. Attenuation of mechanical hypersensitivity by an antagonist of the TRPA1 ion channel in diabetic animals. *Anesthesiology* **111**, 147–154 (2009).
15. Trevisan, G. *et al.* Novel therapeutic strategy to prevent chemotherapy-induced persistent sensory neuropathy by TRPA1 blockade. *Cancer Res.* **73**, 3120–3131 (2013).
16. Oh, M.-H. *et al.* TRPA1-dependent pruritus in IL-13-induced chronic atopic dermatitis. *J. Immunol.* **191**, 5371–5382 (2013).
17. Liu, B. *et al.* TRPA1 controls inflammation and pruritogen responses in allergic contact dermatitis. *FASEB J.* **27**, 3549–3563 (2013).
18. Saccomano, S. J. Acute acetaminophen toxicity in adults. *Nurse Pract.* **44**, 42–47 (2019).
19. Laine, L. *et al.* Double-blind randomized trials of single-tablet ibuprofen/high-dose famotidine vs. ibuprofen alone for reduction of gastric and duodenal ulcers. *Am. J. Gastroenterol.* **107**, 379–386 (2012).
20. De Logu, F. *et al.* The acyl-glucuronide metabolite of ibuprofen has analgesic and anti-inflammatory effects via the TRPA1 channel. *Pharmacol. Res.* **142**, 127–139 (2019).
21. Kokel, D. *et al.* Photochemical activation of TRPA1 channels in neurons and animals. *Nat. Chem. Biol.* **9**, 257 (2013).
22. Lam, P.-Y. *et al.* A high-conductance chemo-optogenetic system based on the vertebrate

channel Trpa1b. *Sci. Rep.* **7**, 11839 (2017).

23. Kokel, D. *et al.* Rapid behavior-based identification of neuroactive small molecules in the zebrafish. *Nat. Chem. Biol.* **6**, 231–237 (2010).
24. Bruni, G., Lakhani, P. & Kokel, D. Discovering novel neuroactive drugs through high-throughput behavior-based chemical screening in the zebrafish. *Front. Pharmacol.* **5**, 153 (2014).
25. McCarroll, M. N., Gendelev, L., Keiser, M. J. & Kokel, D. Leveraging Large-scale Behavioral Profiling in Zebrafish to Explore Neuroactive Polypharmacology. *ACS Chem. Biol.* **11**, 842–849 (2016).
26. Bruni, G. *et al.* Zebrafish behavioral profiling identifies multitarget antipsychotic-like compounds. *Nat. Chem. Biol.* **12**, 559–566 (2016).
27. McCarroll, M. N. *et al.* Zebrafish behavioural profiling identifies GABA and serotonin receptor ligands related to sedation and paradoxical excitation. *Nat. Commun.* **10**, 4078 (2019).
28. Myers-Turnbull, D. *et al.* Simultaneous classification of neuroactive compounds in zebrafish. *bioRxiv* 2020.01.01.891432 (2020) doi:10.1101/2020.01.01.891432.

Chapter 2: Identification of compounds producing non-visual TRPA1-mediated photosensation in zebrafish

ABSTRACT

TRPA1 receptors are important sensors of chemical irritants. In most vertebrates, they do not normally respond to light. Previous studies have identified synthetic photoreactive compounds that confer photosensitivity onto vertebrate TRPA1. However, the pharmacology of TRPA1-mediated non-visual photosensation remains poorly understood. To identify novel compounds that affect this process, we screened a large chemical library for compounds that increased light-elicited motor activity in larval zebrafish. This screen identified structurally diverse hit compounds. A subset of these compounds was photoreactive and produced specific behavioral phenotypes, and a subset of these additionally required functional TRPA1. Together, these studies improve our understanding of non-visual TRPA1-mediated photosensation. In addition, these studies provide novel prototype compounds for controlling TRPA1 with light.

INTRODUCTION

TRPA1 receptors are members of the transient receptor potential (TRP) channel family[1]. They are tetrameric ion channels[2] with cytoplasmic ankyrin repeats that mediate sensitivity to thermal and chemical stimuli[3]. TRPA1 channels respond to a wide variety of reactive compounds including mustard oil[4], industrial electrophiles[5], drug metabolites[6], and other compounds[1,7]. They mediate the inflammatory actions of environmental irritants and proalgesic agents[8]. In addition, they mediate cough[9], inflammation[5], and airway irritation[10]. A gain-of-function mutation in TRPA1 causes familial episodic pain syndrome[11]. These functions are important for diverse animal behaviors.

A relatively small subset of TRPA1 isoforms also respond to light. For example, in specific species of snakes, TRPA1 channels sense infrared light, aiding in prey capture[12]. In human melanocytes, TRPA1 channels respond to UV light, increasing protective pigmentation[13]. Furthermore, TRPA1 homologs are required for extraocular-light avoidance in planaria[14]. Additionally, TRPA1 channels mediate light-induced feeding deterrence[15] and UV light avoidance[16] in *Drosophila*. However, despite these examples, most TRPA1 isoforms, including human and zebrafish isoforms, do not normally respond to light[3].

Understanding TRPA1-mediated photosensation is important for understanding non-visual photo-behaviors. In humans, non-visual photo-behaviors include circadian rhythms, alertness[17], and the pupil reflex[18]. In other species, more diverse non-visual behaviors are observed, including phototaxis in zebrafish[19] and migration in birds[20]. In humans, all visual and non-visual behaviors are mediated by opsins[21]. In non-human species, non-visual behaviors are mediated by at least four additional types of photoreceptors including cryptochromes[22], photoactivated adenylyl cyclases (PACs)[23], gustatory related receptors (GRRs)[24] and TRPA1. TRPA1-mediated non-visual photosensation may represent a potential ancestral function of this gene[14].

Previous studies have identified an exogenous small molecule that enables non-visual TRPA1-mediated photosensation in vertebrates. This small molecule, optovin, is photoactivated by relatively short wavelengths of visible light[25]. Its activity is both light-dependent and rapidly reversible. It acts on various TRPA1 isoforms including human, mouse, and zebrafish[25]. As a result, it enables light-mediated control of transgenic cardiac cells[26] and of endogenous TRPA1-expressing neurons. Optovin's photoactive properties have been linked to its rhodanine ring, a chemical moiety known to absorb light[27]. Several structural analogues of optovin have been identified that also produce similar phenotypes[26]. These data suggest that there may exist other

compounds that are functionally related to optovin that also produce non-visual photosensation via TRPA1.

Despite this progress, few compounds beyond optovin have been identified that activate TRPA1 *in vivo* via photoreactivity. To identify such compounds, we took a behavior-based drug profiling approach in zebrafish. Specifically, we screened a large chemical library for compounds that increased motor activity in response to light stimuli. This screen identified a set of structurally diverse hit compounds that were both photoreactive and produced specific behavioral profiles. A subset of these behavioral phenotypes required functional TRPA1. Together, these data improve our understanding of non-visual photosensation. In addition, they provide structurally diverse prototype compounds that may enable researchers to control endogenous TRPA1 with light.

RESULTS

Optovin produces a distinct behavioral profile

Previous studies of how optovin affects behavior have primarily focused on early stage zebrafish embryos[25]. In embryos, the optovin response includes two spikes of motor activity – a large initial spike followed by a smaller subsequent spike of activity[25]. These motor activity spikes are thought to correspond to C-bend behaviors and swimming behaviors, respectively. However, less is known about optovin activity on zebrafish larvae, which exhibit more complex behaviors than embryos and are a powerful system for studying the vertebrate CNS. Therefore, it is important to characterize optovin activity in zebrafish larvae.

To determine how optovin affects zebrafish larvae, we treated larvae with various TRPA1 ligands, tested them with different stimulus batteries, and analyzed their resulting behavioral profiles. First, larvae were treated with optovin for one hour, and, following a three-minute delay, exposed to a single pulse of light (10 min). Prior to light exposure, the optovin-treated animals demonstrated a significantly lower baseline activity level than DMSO-treated animals. Following activation of the stimulus, the response of optovin-treated animals could be divided into three phases. In the first phase, P1, onset of the stimulus elicited a sharp spike of motor activity, represented as the motion index, or MI (**Fig. 2.1, 2.2**). The MI during this spike increased approximately 8-fold over the optovin baseline (average MI during the pre-stimulus period), and P1 lasted for approximately 6s. (**Fig. 2.1, 2.2, Table 2.1**). In the second phase, P2, motor activity spiked again, increasing approximately 3-fold over the optovin baseline and lasting for approximately 1 minute (**Fig. 2.1, 2.2, Table 2.1**). In the third phase, P3, motor activity remained slightly higher than the optovin baseline for the duration of the stimulus (**Fig. 2.1, 2.2**). Following the stimulus, motor activity reverted to the optovin baseline (**Fig. 2.1, 2.2**). The P1 and P2 motor activity spikes were elicited only by blue (460nm) and violet (395nm) wavelengths, but not by longer wavelengths including green (523nm) and red (660nm) (**Fig. 2.3, 2.4**). Unlike in optovin-treated animals, the P1 and P2 spikes were not observed in control larvae treated with the solvent alone. In P1, the control response only increased 2-fold from the solvent baseline – substantially less than the 8-fold increase observed in optovin-treated animals (**Fig. 2.1, 2.2**). In P2, the control response did not include a broad activity spike, unlike the optovin response. In P3, the control response did not decline (**Fig. 2.1, 2.2**). Another difference was that the control response included a distinct lights-off response at the end of P3 that was not observed in optovin-treated animals (**Fig. 2.1**).

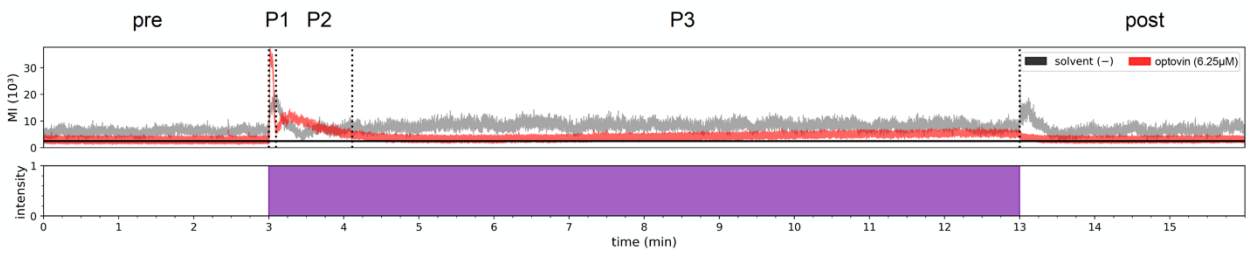

Figure 2.1 Optovin induces a reproducible pattern of behavior
Optovin treated zebrafish exposed to violet light (395nm) display three phases of activity that are distinct from control-treated larvae, shown here in a motor activity plot. Activity is shown as the motion index (MI) on the y-axis, with time on the x-axis. The optovin baseline is indicated by a solid horizontal black line. Phase are delineated by a broken vertical line. Colored bars below the motor activity plot indicate stimuli turning on (colored bar) and off (white bar); colors correspond to stimulus wavelength.

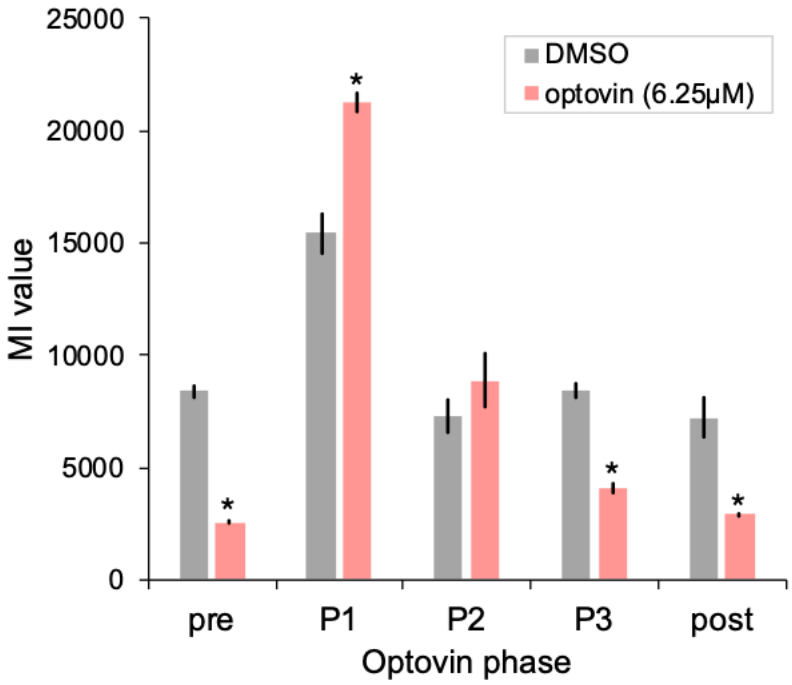

Figure 2.2 The optovin-induced behavior profile is significantly different from the DMSO-induced profile
Bar plot showing average MI values (y-axis) for each optovin phase (x-axis). n = 72 optovin-treated wells (red) and 40 DMSO-treated wells (gray); 8 fish/well. Error bars represent SEM. *p < 0.05.

Table 2.1 Optovin phase data
Details of the optovin phases P1 and P2. P3 not included because it continues through the end of the stimulus (measured up to 10 minutes) and has no peak. n = 72 wells; 8 fish/well.

	Duration (s)	Peak (MI)	Peak time from stimulus start (s)	Peak time from phase start (s)
P1	6.32 ±0.31	40232.49 ±2011.91	1 ±0.06	1 ±0.06
P2	59.93 ±1.42	18113.38 ±2145.06	15.15 ±2.406	8.83 ±2.476

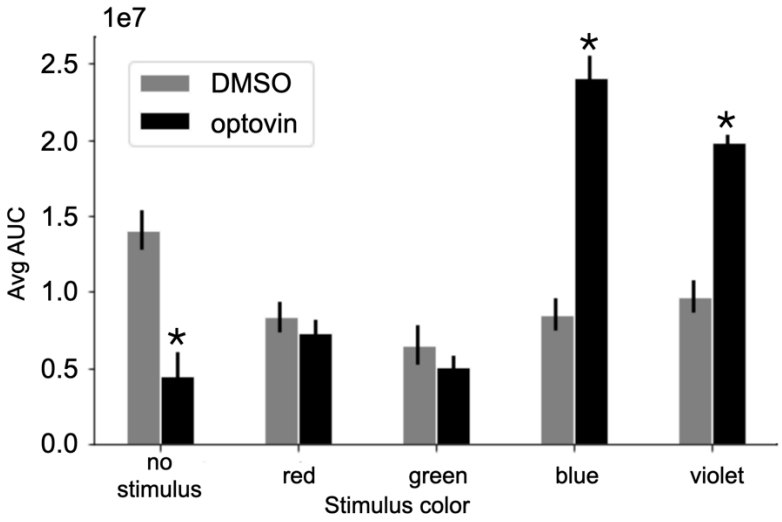

Figure 2.3 Optovin induces the greatest increase in activity in response to blue and violet wavelengths

Bar plot showing AUC (y-axis) of P1 and P2 spikes in optovin- (black) and DMSO- (gray) treated larvae following a 1 minute light stimulus. In optovin treated fish, P1 and P2 motor activity spikes following were elicited only by blue (460nm) and violet (395nm) wavelengths. Red (660nm), green (523nm), and no stimulus conditions did not elicit motor activity. n = 6 wells per stimulus for both optovin and DMSO; 8 fish/well. Error bars represent SEM. *$p < 0.05$.

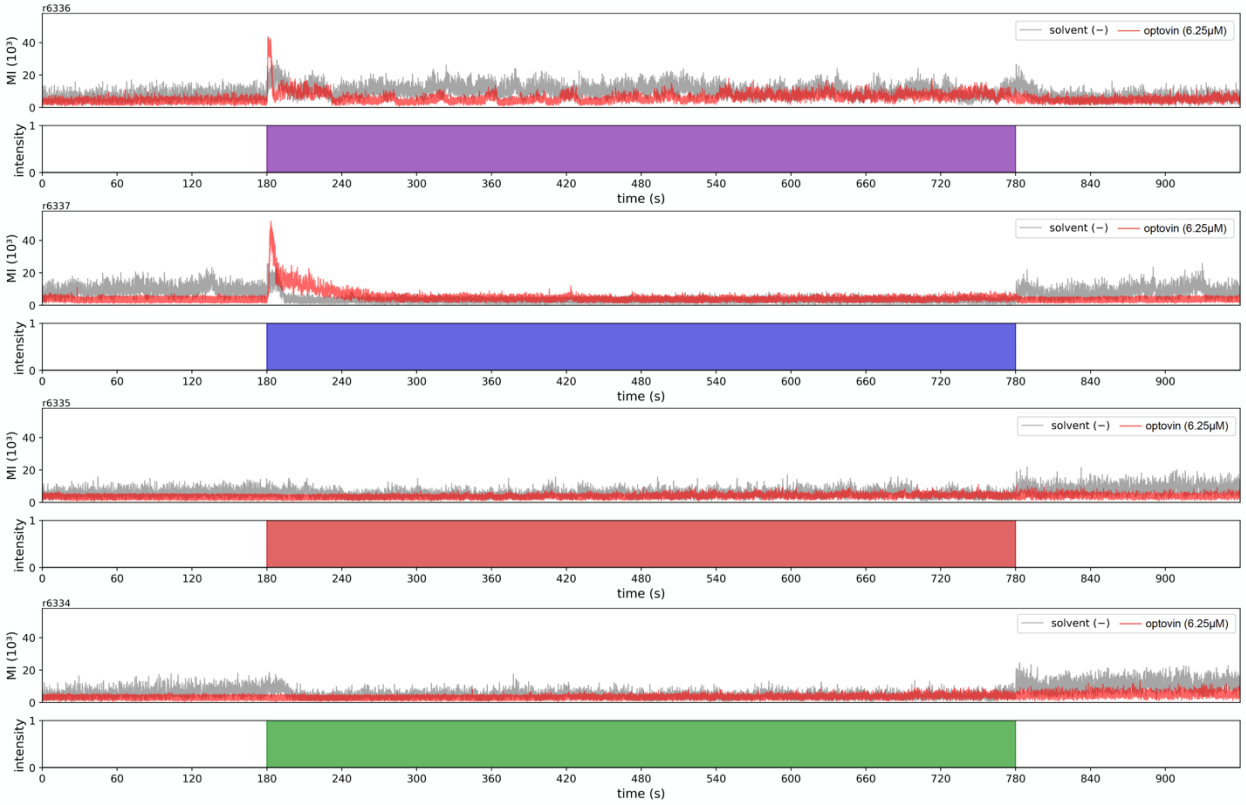

Figure 2.4 Optovin light response to blue, red, and green wavelength stimuli
Motion index traces for 6.25μM optovin-treated larvae exposed to 10 minutes of either violet (395nm), blue (460nm), red (660nm), or green (523nm) light. n = 6 wells per stimulus for both optovin and DMSO; 8 fish/well.

To determine how this optovin response compared to canonical TRPA1 ligands, larvae were treated with allyl isothiocyanate (AITC) and cinnamaldehyde (CA). In optovin-treated animals, multiple stimuli elicited multiple P1 and P2 spikes. By contrast, in neither AITC- nor CA- treated animals did multiple stimuli elicit P1 or P2 spikes (**Fig. 2.5, 2.6**). In both AITC- and CA- treated animals, motor activity increased throughout the assay, including during the P2 phase (**Fig. 2.5**). However, these increases in activity did not resemble the more distinct spikes observed in optovin-treated animals (**Fig. 2.6**). Notably, activity was also increased during the inter-stimulus intervals, whereas in optovin-treated animals activity is greatly decreased between stimuli (**Fig. 2.5, 2.6**). In solvent-treated negative controls, multiple stimuli failed to elicit P1 and P2 spikes (**Fig. 2.6**).

These data suggest that these P1 and P2 motor activity spikes may represent features of a specific behavioral profile that correlates with TRPA1-mediated non-visual photosensation, since these activity spikes specifically occurred in optovin-treated zebrafish larvae but were not observed in untreated larvae, nor in larvae treated with other TRPA1 ligands, such as AITC and CA. Alternatively, this behavioral profile may be a random coincidence with little predictive power for identifying novel TRPA1 ligands. To distinguish between these alternatives, we analyzed a larger number of compounds.

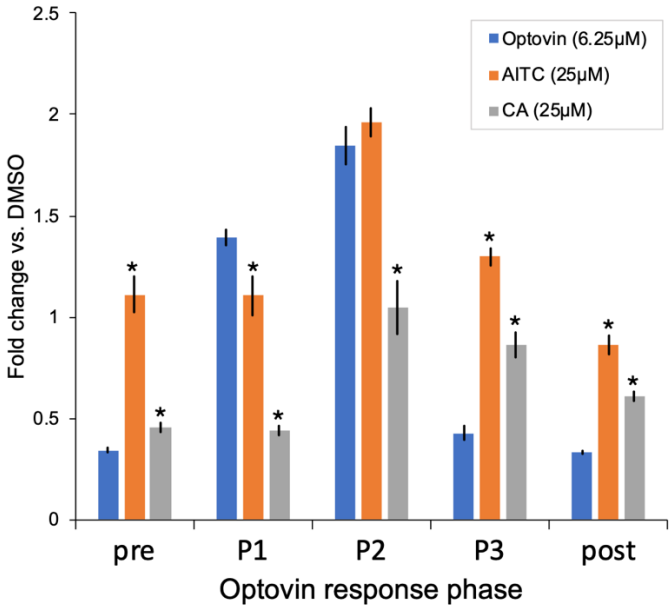

Figure 2.5 The optovin-induced behavioral profile differs from the behavioral profiles induced by known TRPA1 ligands
Bar plot showing activity fold change vs. DMSO (y-axis) of optovin- (blue), allyl isothiocyanate- (AITC, orange), and cinnamaldehyde- (CA, gray) treated larvae during each of the optovin-defined phases (x-axis). n = 8 wells per treatment; 8 fish/well. Error bars represent SEM.*p < 0.05.

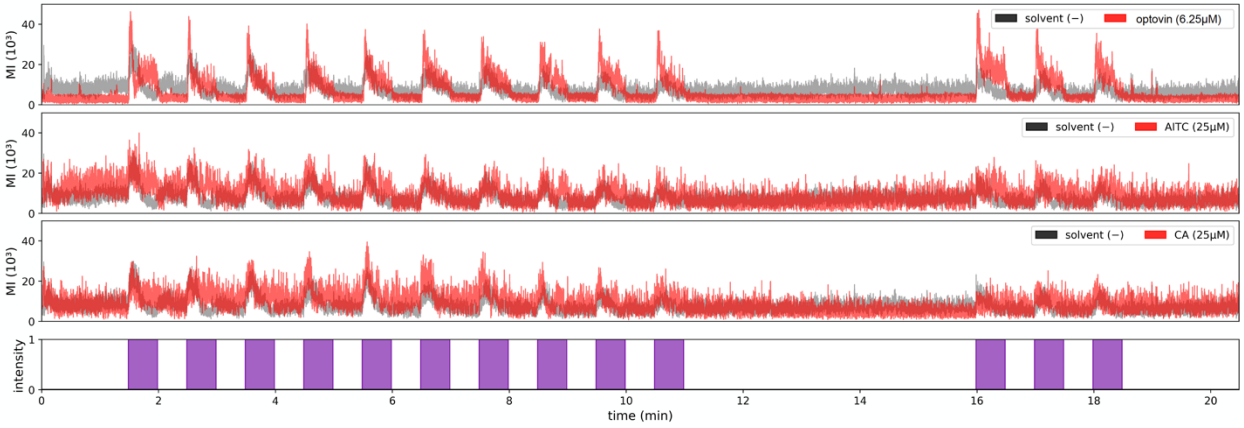

Figure 2.6 MI traces illustrate difference between optovin-, AITC-, and CA-induced behavior
Representative activity traces for larvae treated with the indicated compounds (red) or control (grey). AITC, allyl isothiocyanate; CA, cinnamaldehyde. n = 3 wells per treatment; 8 fish/well.

Large-scale chemical screening

In previous studies, large-scale behavior based chemical screens in zebrafish have successfully identified diverse classes of neuroactive compounds related to anesthesia[28], sleep[29], fear[30], feeding[31], and antipsychotics[32]. Despite this progress, it remains unclear if novel compounds that produce TRPA1-mediated non-visual photo sensation can be identified based on their behavioral profiles. To answer this question, we analyzed behavioral data collected from a large-scale chemical screen (**Fig. 2.7**).

In this screen, the chemical library included 30,656 structurally diverse compounds. These compounds were profiled on zebrafish larvae using a battery of behavioral phenotyping assays that included a variety of stimuli, including light-based stimuli. The primary screening hits, defined as any compound that substantially increased motor activity in response to light**,** comprised 269 potential hit compounds including 54 false positive solvent-treated controls (**Fig. 2.8**). These potential hits were manually reviewed to prioritize the most promising hit compounds and remove false positives due to camera flickers and other technical errors, yielding 99 primary hits (**Fig. 2.7**). From these hits, 6 optovin analogues were removed, and a subset of 93 primary hits were reordered and retested (**Fig. 2.7**). Of these 93 primary hit compounds, 34 (36.56%) reproducibly increased light-induced motor activity in vivo, and 17 compounds were selected as final hits following dose-response testing. An additional four compounds were included based on manual analysis identifying them as potential hits of interest for a final total of 21 hit compounds (**Fig. 2.9, 2.7**).

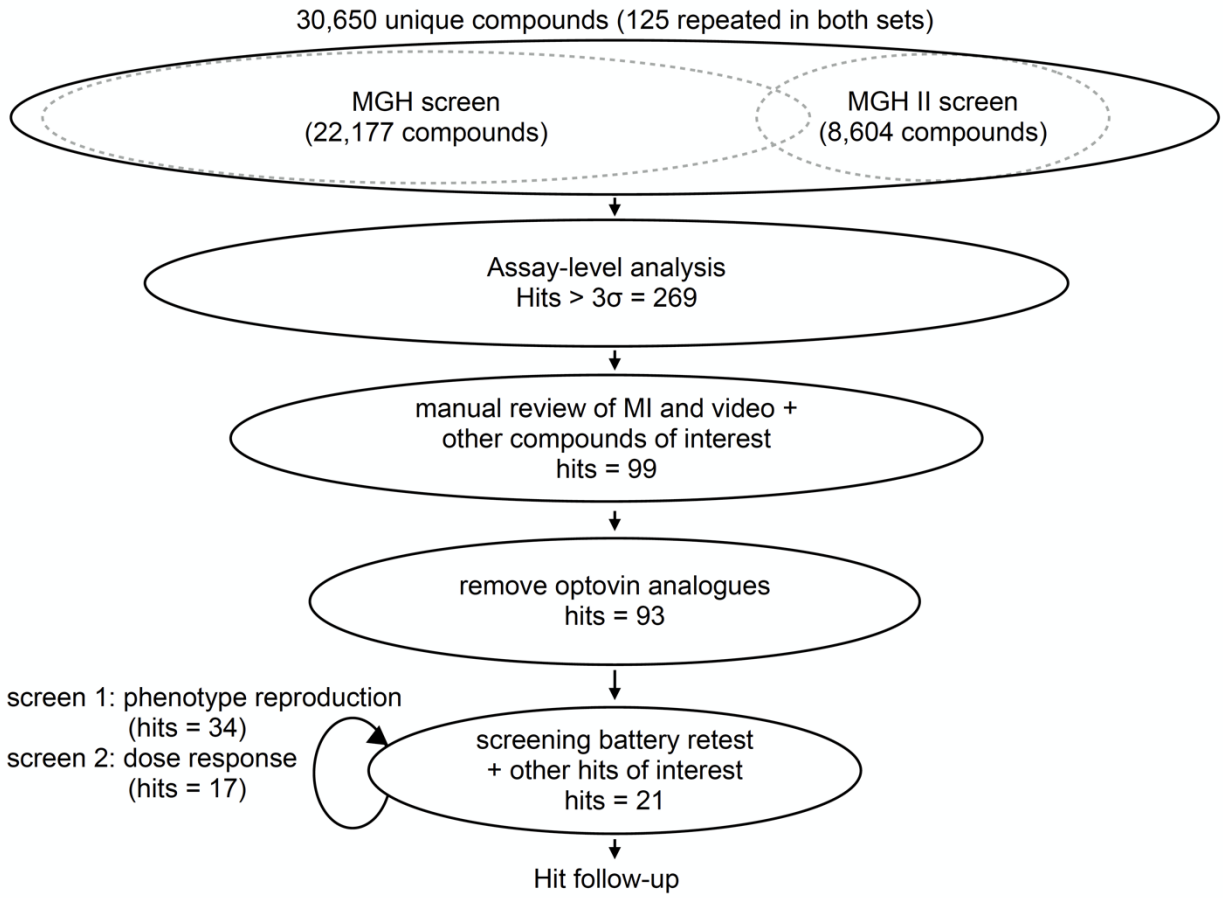

Figure 2.7 Hit screening and identification process
Flowchart depicting the process of testing, screening, and identifying final set of hit compounds. Hits listed within each level represents the resulting number of hits from that level.

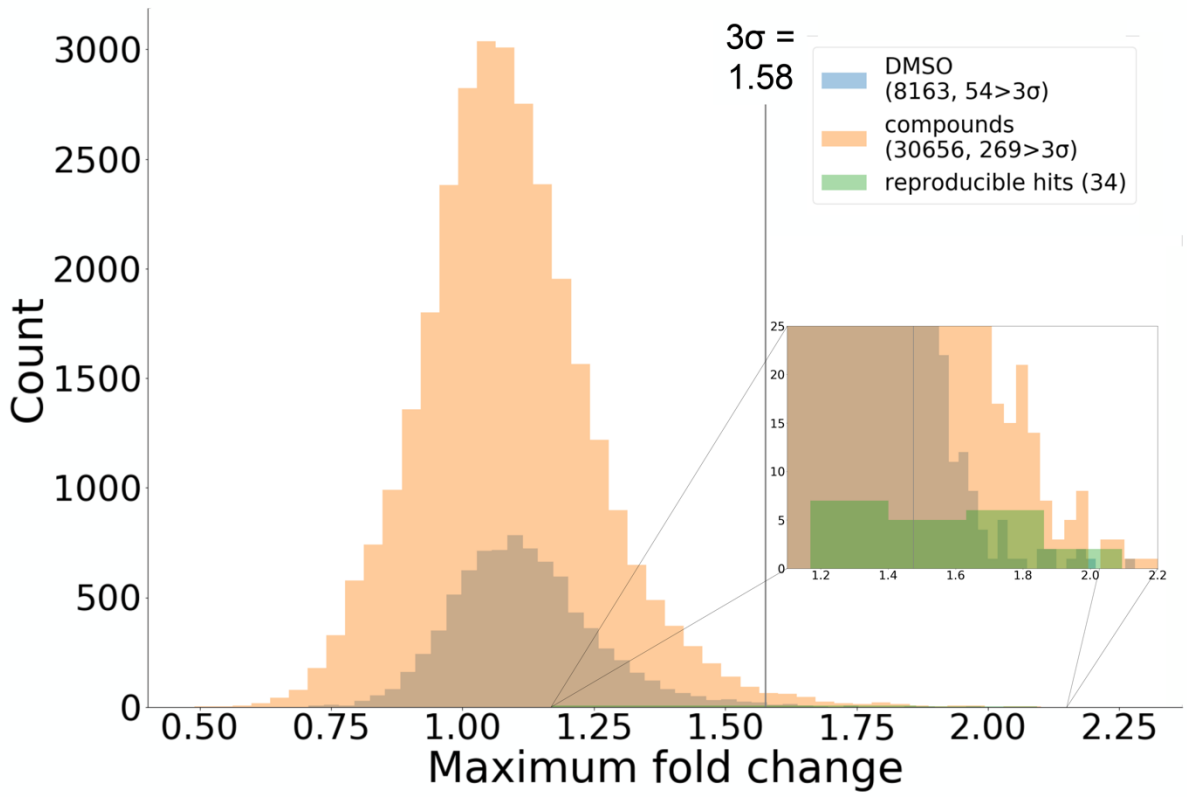

Figure 2.8 Large-scale screening identifies early hit compounds
Two chemical libraries, containing a combined 30,656 structurally diverse compounds and 8,163 negative DMSO controls, were tested against a battery containing a variety of light-based stimuli. Fold change in activity versus DMSO was calculated for each compound for stimuli of interest. Compounds that had at least one measured value with a fold change greater than 3σ (1.58) were selected for further retesting, from which 34 were selected for dose-response testing. n = 1 well per compound and 8163 wells DMSO; 8 fish/well.

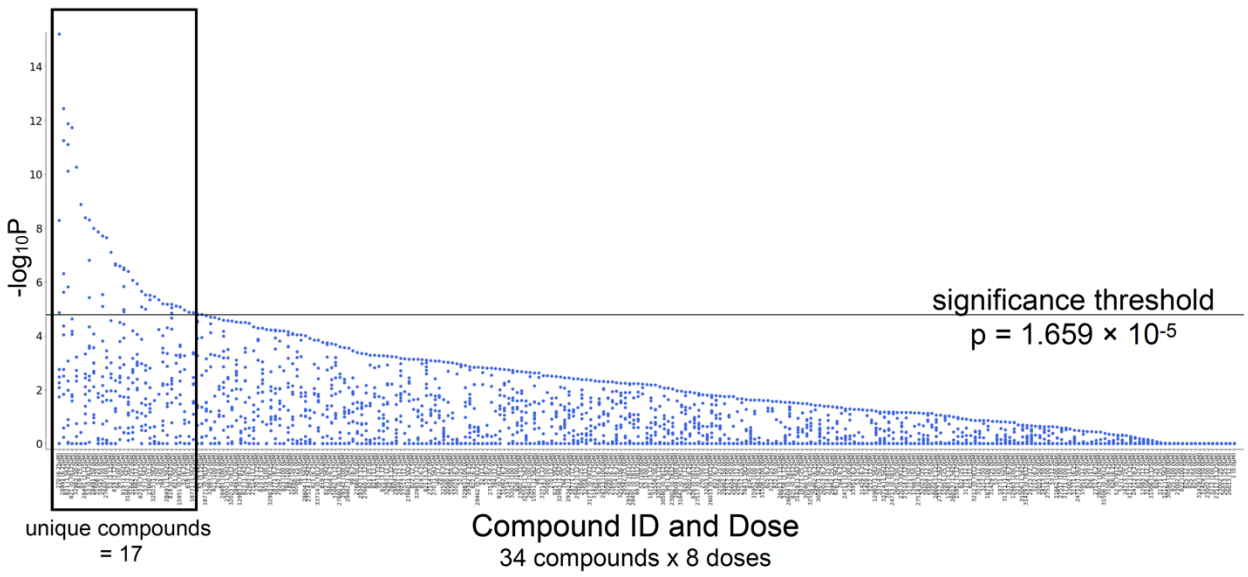

Figure 2.9 Dose-response analysis finalizes hit set and identifies optimal doses
Scatter plot showing $-\log_{10}P$ values for selected stimuli of interest for each compound-treated well compared against the corresponding stimulus in DMSO-treated wells. The 34 compounds selected for dose-response analysis were tested at 2-fold intervals from 0.78125μM to 100μM against the screening battery. Seventeen unique compounds exceeded the significance threshold (horizontal line). n = 6 wells/test compound/dose, 368 wells DMSO, 118 wells optovin, and 96 wells with no treatment; 8 fish/well. Significance threshold corrected using Bonferroni.

Structural analyses revealed that the validated hit compounds included a wide variety of structures. These compounds clustered into at least 11 structural classes (**Fig. 2.10, 2.11, Table 2.2**). Unlike optovin, most of the novel hit compounds did not contain a rhodanine ring except compound 784. However, there were several other features of note. Though they did not cluster together, compounds 15951 (cluster 10) and 23002 (cluster 2) both have an adamantane group. Additionally, compounds 819 and 825 in cluster 5 both have a central, fused double thiazole along with distinct symmetry in each compound. Likewise, compounds in cluster 6 all share a thienopyridine. Together, these data suggest that, like optovin, a subset of these novel compounds may also be photoactivated TRPA1 ligands, as the validated hit compounds reproducibly produce light-elicited behavioral excitation. Interestingly, the hit compounds included a variety of chemical structures, raising questions about their potential mechanisms of action and photoreactivity.

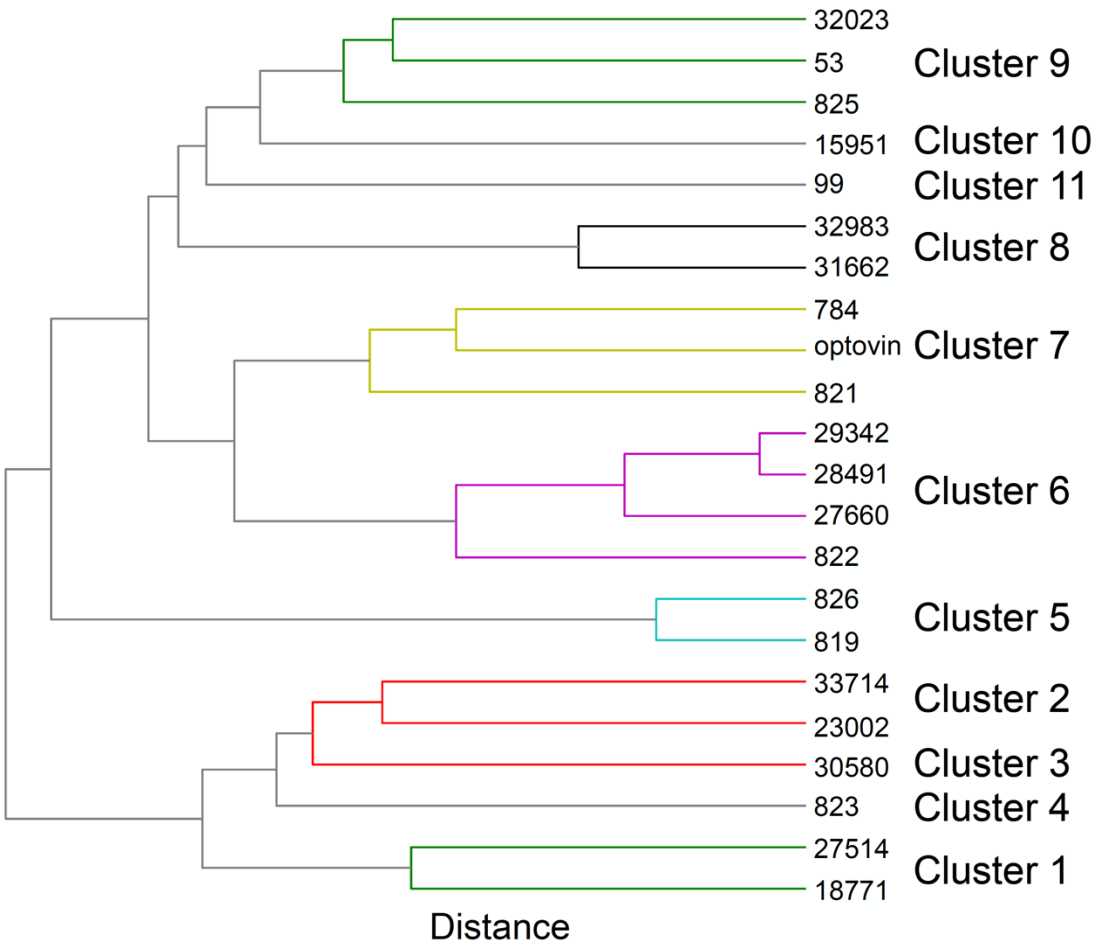

Figure 2.10 Hierarchical clustering identifies 11 structural classes
Dendrogram depicting hierarchical clustering of hit compound structures.

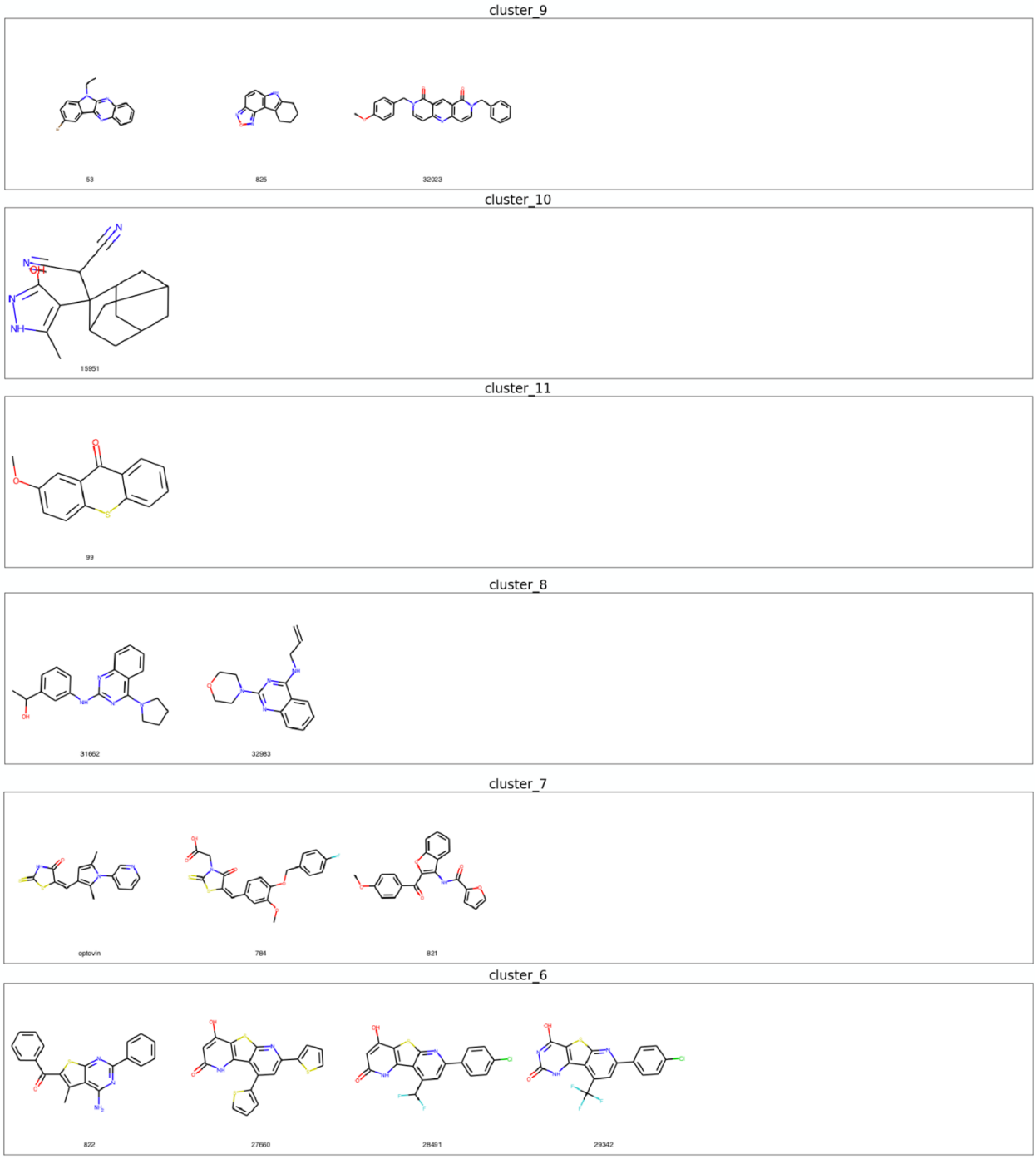

Figure 2.11 Hit compound structures grouped by cluster
Hit compound structures grouped by clusters identified via hierarchical clustering (cont'd on following page)

Figure 2.11 Hit compound structures grouped by cluster (cont'd)

Table 2.2 Hit compound SMILES

Compound ID	SMILES
optovin	Cc1cc(C=C2SC(=S)NC2=O)c(C)n1-c1cccnc1
53	CCn1c2ccc(Br)cc2c2nc3ccccc3nc21
99	COc1ccc2sc3ccccc3c(=O)c2c1
784	COc1cc(ccc1OCc2ccc(cc2)F)/C=C/3\C(=O)N(C(=S)S3)CC(=O)O
819	c12c(nc(s2)c2cc(c(O)cc2)OC)sc(n1)c1cc(OC)c(cc1)O
821	COc1ccc(cc1)C(=O)c2c(c3ccccc3o2)NC(=O)c4ccco4
822	Cc1c2c(nc(nc2sc1C(=O)c3ccccc3)c4ccccc4)N
823	CCN(CC)c1ccc(cc1)n2nc3cc(c(cc3n2)N)C
825	c1cc2c(c3c1[nH]c4c3CCCC4)non2
826	c12c(nc(s2)c2ccc(cc2)CC)sc(n1)c1ccc(cc1)CC
15951	Cc1[nH]nc(O)c1C1(C(C#N)C#N)C2CC3CC(C2)CC1C3
18771	O=C(CN1CCCCC1)Nc1cc(Cl)cc(Cl)c1
23002	O=C(Nc1ccc2c(c1)COC2=O)C12CC3CC(CC(C3)C1)C2
27514	O=C(Nc1ccc(Cl)c(Cl)c1)N1CCN(C2CCSCC2)CC1
27660	O=c1cc(O)c2sc3nc(-c4cccs4)cc(-c4cccs4)c3c2[nH]1
28491	O=c1cc(O)c2sc3nc(-c4ccc(Cl)cc4)cc(C(F)F)c3c2[nH]1
29342	O=c1nc(O)c2sc3nc(-c4ccc(Cl)cc4)cc(C(F)(F)F)c3c2[nH]1
30580	COc1ccccc1NC(=O)N1CCCC1c1ccc(Cl)cc1
31662	CC(O)c1cccc(Nc2nc(N3CCCC3)c3ccccc3n2)c1
32023	COc1ccc(Cn2ccc3nc4ccn(Cc5ccccc5)c(=O)c4cc3c2=O)cc1
32983	C=CCNc1nc(N2CCOCC2)nc2ccccc12
33714	CSc1ccccc1NC(=O)C1(c2ccccc2)CCOCC1

Photoactivity of hit compounds greatly varies

Previous studies have revealed that aspects of TRPA1-mediated photo-sensation involve photoreactivity. For example, TRPA1 is activated by photosensitizing agents *in vitro*[33]. Furthermore, optovin is a photoreactive compound[25]. Thus, we hypothesized that a subset of hit compounds would also be photoreactive. To answer this question, we measured a variety of photochemical properties including their absorbance, photostability after multiple irradiations, fluorescence, and phototoxicity.

The absorbance studies revealed that most compounds displayed peak absorbance between wavelengths ~310 and 410nm (**Fig. 2.12, 2.13**). For example, 99, 784, and 28491 displayed peak absorbance at 390nm, 410nm, and 350nm, respectively (**Fig. 2.12, 2.13**). Several compounds produced two absorbance peaks including 53, 825, and 27660 (**Fig. 2.12, 2.13**). By contrast, none of the novel hit compounds had a maximum absorbance above 410nm (**Fig. 2.12, 2.13**), while six compounds (15951, 18771, 27514, 30580, 31662, 33714) did not display absorbance at any wavelength tested. Optovin absorbance, by comparison, occurs at 470nm, which is an outlier compared to the absorption range of the hit compounds (**Fig. 2.12, 2.13**). The DMSO-treated negative controls displayed no absorption at any wavelength in the tested range (**Fig. 2.12, 2.13**).

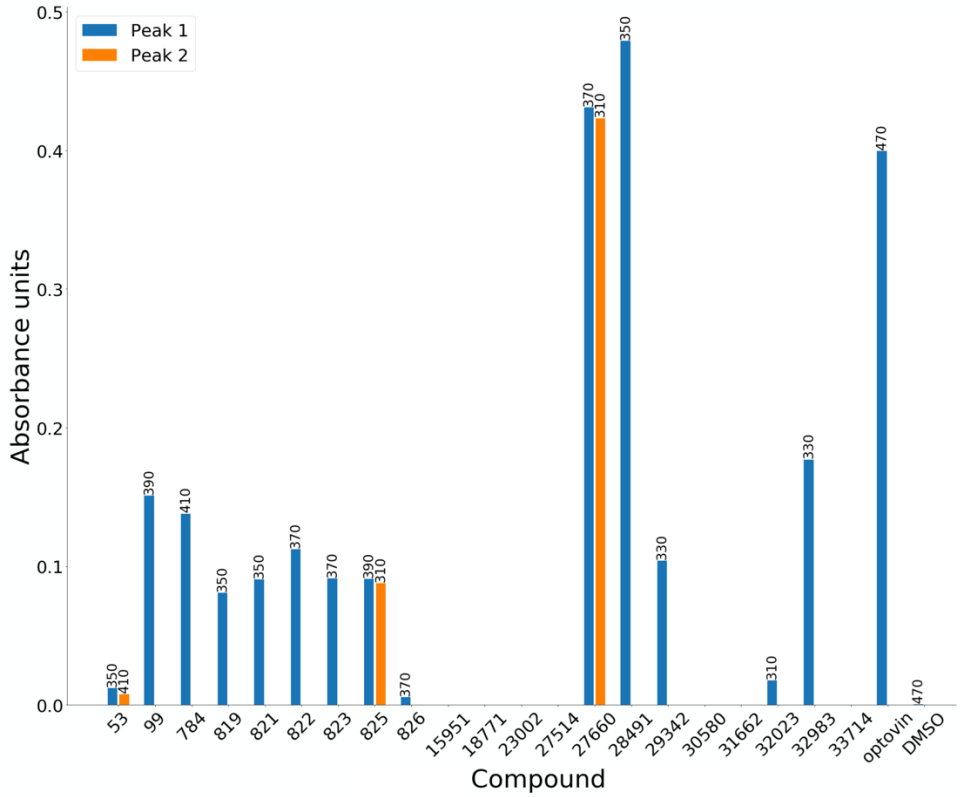

Figure 2.12 Hit compound absorbance
Bar plot showing the magnitude (y-axis) of light absorbance of hit compounds. Where more than one absorbance peak was detected, the bar for the secondary peak is colored in orange. Absorbance wavelengths (nm) are labeled at the top of each bar.

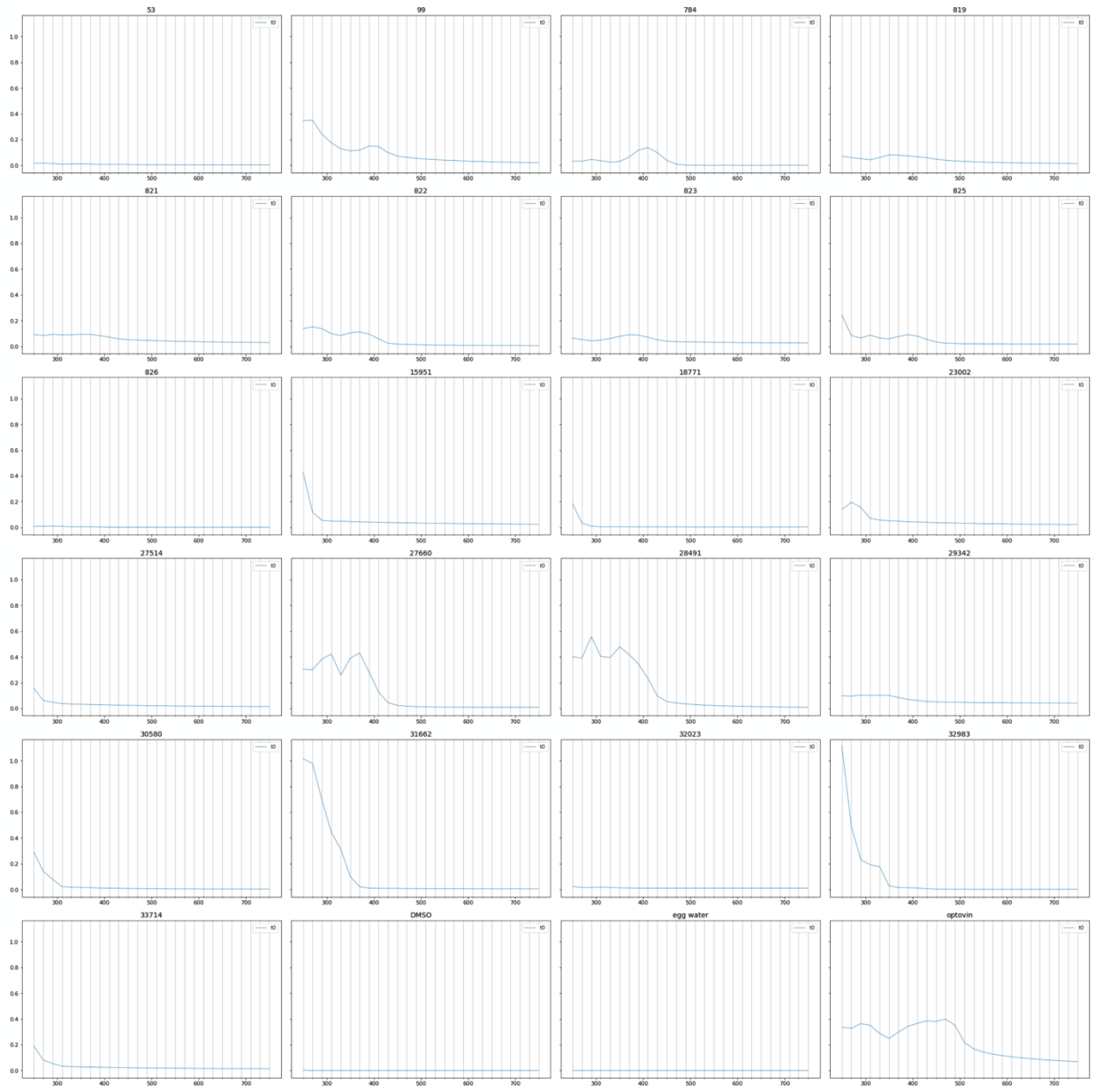

Figure 2.13 Hit compound raw absorbance data
Absorbances (measured in absorbance units) of hit compounds dissolved in egg water.

As a measure of photostability, we determined if the compounds changed absorbance after multiple irradiations. In 17 of 21 hit compounds, the maximum change in absorbance was equal to or less than 0.10 absorbance units, a change that was relatively minor (**Fig. 2.14, 2.15, Table 2.3**). For example, 7 compounds (including 53, 784, 825, 15951, 18771, 23002, 29342) increased absorbance by 0.10 absorbance units or less (**Fig. 2.14, 2.15, Table 2.3**). Similarly, 10 compounds (including 99, 819, 821, 823, 826, 27514, 30580, 32032, 32983, 33714) decreased absorbance by less than 0.10 absorbance units (**Fig. 2.14, 2.15, Table 2.3**). By contrast, multiple irradiations greatly increased the absorbance of compounds 28491 and 31662, rising by 0.55 and 0.34 absorbance units, respectively, while absorbance in compounds 822 and 27660 was reduced by 0.11 and 0.14, respectively (**Fig. 2.14, 2.15, Table 2.3**). Comparatively, the 0.12 absorbance unit reduction of peak absorbance in optovin occurred at 470nm, while DMSO demonstrated no change (**Fig. 2.14, 2.15, Table 2.3**).

Fluorescence studies revealed that most hit compounds were not strongly fluorescent (**Table 2.4**). For example, 14 compounds (53, 784, 819, 825, 826, 15951, 18771, 23002, 27514, 29342, 30580, 32023, 32983, 37714) had excitation/emission wavelengths of 350nm/395nm (**Table 2.4**). By contrast, a subset of compounds showed measurable emissions. For example, compounds 821 and 822 emitted in the blue range (455nm and 475nm, respectively) (**Table 2.4**). Compounds 99, 823, 27660 (all 535nm) and 28491 (515nm) emitted in the green range (**Table 2.4**). One outlier was compound 99, which displayed a maximum excitation wavelength at 410 nm (**Table 2.4**). Importantly, neither optovin nor DMSO were strongly fluorescent, displaying maximum excitation/emission at 350nm/395nm (**Table 2.4**).

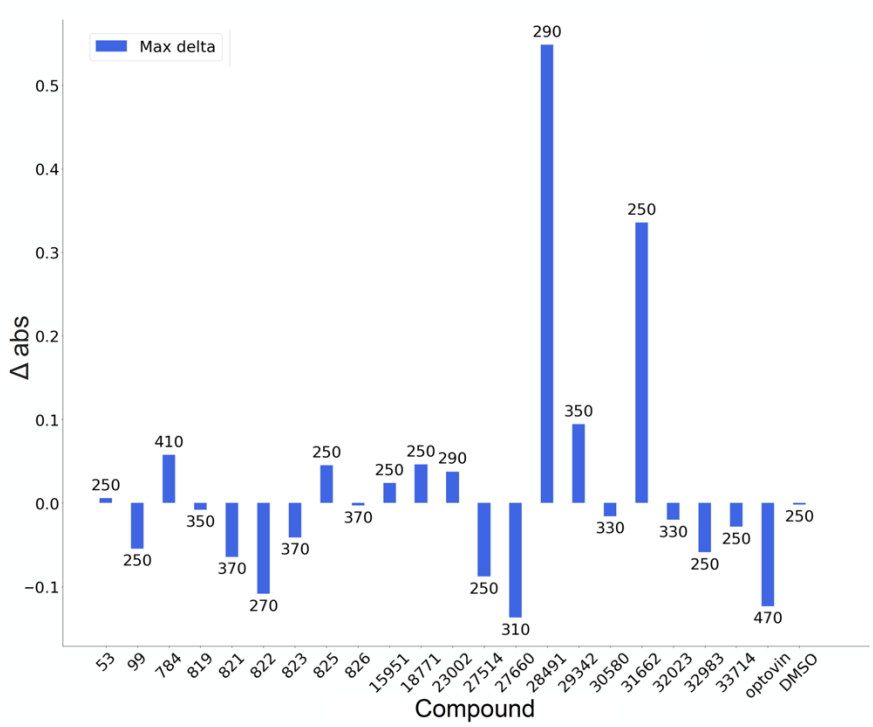

Figure 2.14 Changes in hit compound absorbance following exposure to violet light
Bar plot showing the maximum change in absorbance (y-axis) following multiple irradiation. Following an initial baseline absorbance measurement, compounds were exposed to violet light for varying lengths of time between 5 and 1200s (20 min.), after which absorbance was measured again. Max delta refers to the greatest change in absorbance at one wavelength between any two timepoints. Absorbance wavelengths (nm) are labeled at the top of each bar.

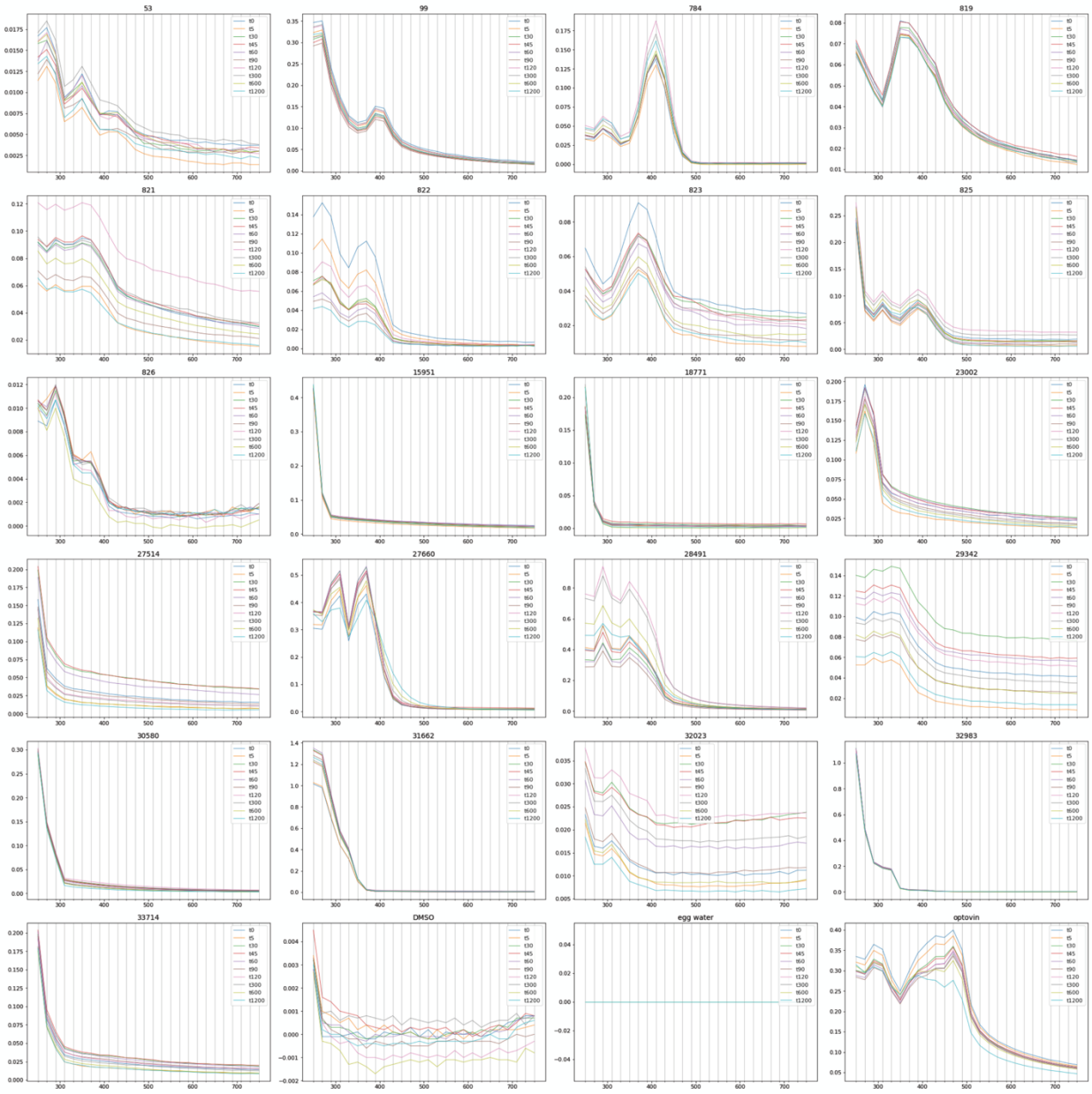

Figure 2.15 Hit compound raw absorbance data following multiple irradiation
Absorbances (measured in absorbance units) of hit compounds dissolved in egg water. Following an initial baseline absorbance measurement, compounds were exposed to violet light for varying lengths of time between 5 and 1200s (20 min.), after which absorbance was measured again.

Table 2.3 Values for max delta following multiple irradiation
Actual values for max delta as shown in Fig. 2.14. Max delta refers to the greatest change in absorbance at one wavelength between any two timepoints. Change is calculated using the earlier timepoint as a baseline.

Compound ID	Max delta	Wavelength (nm)
53	0.0057	250
99	-0.0546	250
784	0.0577	410
819	-0.0078	350
821	-0.0643	370
822	-0.1086	270
823	-0.041	370
825	0.0451	250
826	-0.0029	370
15951	0.0239	250
18771	0.0463	250
23002	0.0377	290
27514	-0.0878	250
27660	-0.137	310
28491	0.5482	290
29342	0.0943	350
30580	-0.0156	330
31662	0.3354	250
32023	-0.02	330
32983	-0.0588	250
33714	-0.0283	250
optovin	-0.1233	470
DMSO	-0.0018	250

Table 2.4 Excitation/emissions experiments showed that most compounds are not strongly fluorescent

For each compound, the maximum excitation and emission wavelengths were identified. Outliers that excite/emit at wavelengths other than 350nm/395nm are highlighted in red.

Compound ID	Excitation wavelength	Emission wavelength
53	350	395
99	410	535
784	350	395
819	350	395
821	390	455
822	390	475
823	350	535
825	350	395
826	350	395
15951	350	395
18771	350	395
23002	350	395
27514	350	395
27660	370	535
28491	350	515
29342	350	395
30580	350	395
31662	350	395
32023	350	395
32983	350	395
33714	350	395
Optovin	350	395
DMSO	350	395

As another measure of photoreactivity, we determined if the compounds produced phototoxicity. To this end, we tracked the activity of treated fish for 12 hours. During the first six, larvae were exposed to light stimulus, after which activity was tracked for an additional six hours. Length of survival/time of death was calculated quantitatively by analysis of the MI traces. These phototoxicity studies revealed that many of the hit compounds (12/21) demonstrated some level of phototoxicity under violet and blue wavelengths (**Fig. 2.16, Table 2.5, 2.6**). For example, four compounds (including 53, 27660, 28491, and 29342) were significantly phototoxic under both violet and blue wavelengths, and seven compounds (including 99, 819, 821, 822, 823, 826, 32983) were significantly phototoxic under only violet wavelengths. Other compounds demonstrated a trend towards phototoxicity, though not at significant levels. These include 99 and 819, which have some blue wavelength toxicity in addition to their violet wavelength toxicity, and 32023, which has only blue wavelength toxicity (**Fig. 2.16, Table 2.5, 2.6**). Additionally, two compounds (53 and 28491) showed a dose-dependent sensitivity to different wavelengths, with higher doses conferring phototoxicity under both violet and blue wavelengths, while lower doses conferred phototoxicity only in the presence of violet wavelengths (**Fig. 2.16, Table 2.5, 2.6**). Phototoxicity most often occurred within the first two hours of light exposure and death rarely occurred under the green, red, or no stimulus conditions (**Fig. 2.16, Table 2.5, 2.6**). While some fish did die under red and green light conditions, these tended to be single replicates, and death occurred relatively late in the experiment (>8 hours). Two compounds (30580 and 33714) were significantly toxic under all conditions, including when no stimulus was present, while another two, 15951 and 31662, trended towards general toxicity. Interestingly, in compound 30580, which was shown to be generally toxic, the presence of red light significantly increased survival above the no stimulus condition (**Fig. 2.16, Table 2.5, 2.6**). A small number of hit compounds (5 out of 21) were not phototoxic under any conditions including 784, 825, 18771, 23002, and 27514. Likewise, optovin and low dose (25μM and 100μM) eugenol were not phototoxic, though optovin demonstrated a slight trend towards phototoxicity under violet wavelengths.

Importantly, solvent-treated negative controls were not toxic under any conditions, independent of stimulus wavelength. Furthermore, eugenol-treated (300μM) positive controls were toxic under all conditions, independent of stimulus wavelength (**Fig. 2.16, Table 2.5, 2.6**).

Together, these photoreactivity data suggest that although a subset of hit compounds were photoreactive, this photoreactivity was difficult to measure by absorbance, multiple irradiation, and fluorescence. However, most of the hit compounds were phototoxic to some degree. These data suggest that many of the hit compounds are photoreactive, raising questions about their target and phenotypic specificity.

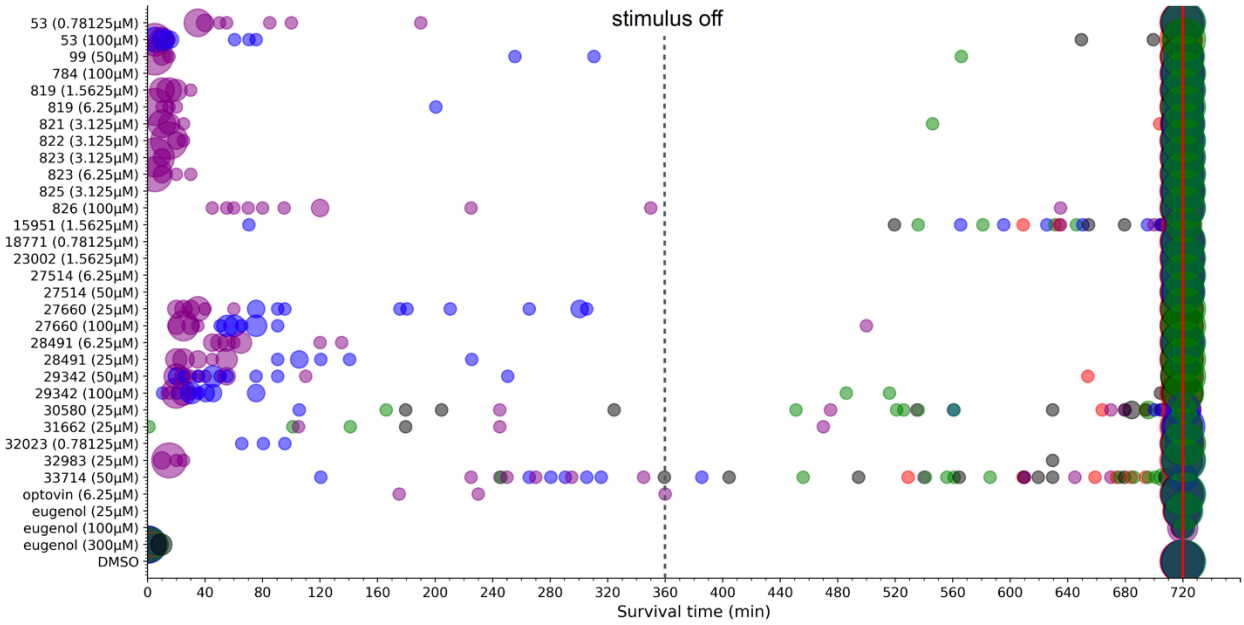

Figure 2.16 Survival time following hit compound treatment and exposure to varying light wavelengths

Plot depicting the survival time of hit compound-treated larvae exposed to varying wavelengths of light. The activity of treated fish was tracked for 12 hours. During the first six, larvae were exposed to light stimulus, after which activity was tracked for an additional six hours. Marker color indicates stimulus wavelength (no stimulus condition indicated by black). The size of the marker indicates the number of wells, with the position of the marker along the x-axis indicating the time at which those wells were considered to have died. Time of death was determined by identifying the last 5 minute window in which the standard deviation of activity was equal to or less than the overall standard deviation of activity in the 300μM eugenol-treated positive controls. Wells that did not meet this criterion within the 12 hour period were considered to have survived. n = 12 wells per stimulus per compound; 8 fish/well.

Table 2.5 Length of survival with exposure to light
Average length of survival (min.) during the phototoxicity experiment described in Fig. 2.16. n = 12 wells per stimulus per compound; 8 fish/well. *p < 0.05.

Compound ID	Violet	Blue	Red	Green	No stimulus	Group
53 (0.78125μM)	61* ±13.24	720	720	720	720	B
53 (100μM)	8* ±0.97	24* ±7.88	720	720	713 ±5.92	A
99 (50μM)	7* ±0.94	647 ±49.28	720	707 ±12.92	720	A
784 (100μM)	720	720	720	720	720	A
819 (1.5625μM)	16* ±1.72	720	720	720	720	A
819 (6.25μM)	8* ±1.44	677 ±43.33	720	720	720	A
821 (3.125μM)	190* ±92.27	720	719 ±1.25	705 ±14.58	720	B
822 (3.125μM)	17* ±0.94	720	720	720	720	B
823 (3.125μM)	6* ±0.56	720	720	720	720	B
823 (6.25μM)	9* ±2.29	720	720	720	720	A
825 (3.125μM)	720	720	720	720	720	B
826 (100μM)	215* ±67.42	720	720	720	720	B
15951 (1.5625μM)	710 ±7.1	625 ±52.91	704 ±11.06	679 ±18.98	693 ±16.86	C
18771 (0.78125μM)	720	720	720	720	720	C
23002 (1.5625μM)	720	720	720	720	720	C
27514 (6.25μM)	720	720	720	720	720	D
27514 (50μM)	719 ±0.83	720	720	719 ±0.83	720	D
27660 (25μM)	33* ±3.11	233* ±51.38	720	720	720	B
27660 (100μM)	65* ±39.53	65* ±3.4	720	720	720	B
28491 (6.25μM)	68* ±8.4	720	720	720	720	B
28491 (25μM)	35* ±4.15	425* ±89.33	720	720	720	B
29342 (50μM)	38* ±7.52	63* ±18.04	715 ±5.42	720	720	B
29342 (100μM)	22* ±1.14	40* ±5.59	720	683 ±24.79	719 ±1.25	B
30580 (25μM)	637 ±42.77	653 ±51.48	713* ±4.86	585 ±47.89	579* ±60.79	D
31662 (25μM)	608 ±62.57	720	720	560 ±84.03	675 ±45	D
32023 (0.78125μM)	720	560 ±83.58	720	720	720	B
32983 (25μM)	15* ±1.14	720	720	720	713 ±7.5	B
33714 (50μM)	461 ±59.32	463 ±67.61	681 ±16.89	592 ±39.66	602* ±35.74	D
optovin (6.25μM)	604 ±0	720	720	720	720	A
eugenol (25μM)	720	720	720	720	720	--
eugenol (100μM)	720	720	720	720	720	--
eugenol (300μM)	1 ±0.65	1 ±0.65	2 ±0.71	2 ±0.71	3* ±1.31	--
DMSO	720 ±61.83	720	720	720	720	--

Table 2.6 P-values for length of survival with exposure to light

P-values for the average length of survival (min.) during the phototoxicity experiment described in Fig. 2.16. For the violet, blue, red, and green conditions, p-values were calculated using the same compound with no stimulus exposure as the control. For the no stimulus condition, p-values were calculated versus DMSO with no stimulus exposure as the control. A p-value of 0 indicates no difference from the control. n = 12 wells per stimulus per compound; 8 fish/well.

Compound ID	Violet	Blue	Red	Green	No stimulus (vs DMSO)	Group
53 (0.78125μM)	2.67E-14	0	0	0	0	B
53 (100μM)	3.36E-19	8.92E-26	0.231308	0.231308	0.231308	A
99 (50μM)	2.62E-27	0.167004	0	0.338801	0	A
784 (100μM)	0	0	0	0	0	A
819 (1.5625μM)	2.36E-24	0	0	0	0	A
819 (6.25μM)	2.96E-25	0.338801	0	0	0	A
821 (3.125μM)	0.000129499	0	0.338801	0.338801	0	B
822 (3.125μM)	3.06E-27	0	0	0	0	B
823 (3.125μM)	8.97E-30	0	0	0	0	B
823 (6.25μM)	4.85E-23	0	0	0	0	A
825 (3.125μM)	0	0	0	0	0	B
826 (100μM)	1.2E-05	0	0	0	0	B
15951 (1.5625μM)	0.376838	0.242708	0.611412	0.582503	0.142008	C
18771 (0.78125μM)	0	0	0	0	0	C
23002 (1.5625μM)	0	0	0	0	0	C
27514 (6.25μM)	0	0	0	0	0	D
27514 (50μM)	0.338801	0	0	0.338801	0	D
27660 (25μM)	2.02E-21	1.25E-06	0	0	0	B
27660 (100μM)	4E-09	9.08E-21	0	0	0	B
28491 (6.25μM)	2.02E-16	0	0	0	0	B
28491 (25μM)	5.02E-20	0.0071086	0	0	0	B
29342 (50μM)	3.67E-17	8.06E-13	0.338801	0	0	B
29342 (100μM)	6.01E-44	6.41E-20	0.338801	0.18124	0.338801	B
30580 (25μM)	0.445117	0.367518	0.0497961	0.936401	0.0408208	D
31662 (25μM)	0.397289	0.338801	0.338801	0.244318	0.338801	D
32023 (0.78125μM)	0	0.0819291	0	0	0	B
32983 (25μM)	7.35E-18	0.338801	0.338801	0.338801	0.338801	B
33714 (50μM)	0.0569664	0.087651	0.0628211	0.853166	0.0070885	D
optovin (6.25μM)	0.0867941	0	0	0	0	A
eugenol (25μM)	0	0	0	0	0	--
eugenol (100μM)	0	0	0	0	0	--
eugenol (300μM)	0.404312	0.404312	0.582379	0.582379	9.09E-26	--
DMSO (1μM)	0	0	0	0	N/A	--

Hit compounds cluster into four phenotypic classes

Previous research has shown that compounds with similar behavioral profiles tend to act via similar molecular mechanisms, a key principle of phenotype based genetic screens[34]. Therefore, we wondered if the hit compounds produced distinct behavioral sub-classes. To answer this question, we analyzed their behavioral profiles using a multi-step process. First, optimal doses for each compound were selected by identifying the concentration of each compound that produced the maximum increase in motor activity (**Fig. 2.9**). At this optimal concentration, all the hits were then tested in a behavioral battery designed to emphasize potential phenotypic differences. To visualize these differences, the behavioral profiles were analyzed by tSNE (**Fig. 2.17**) and pairwise clustering (**Fig. 2.18**), then inspected by a manual analysis (**Fig. 2.19, 2.20**).

These analyses revealed that the behavioral profiles could be classified into four main groups (Groups A-D), with DMSO-treated negative control wells clustered in a fifth group. The first group, Group A, included optovin and 4 additional compounds (53, 99, 784, 819) (**Fig. 2.21, 2.22, Table 2.7**). These compounds produced phenotypes similar to the optovin response, characterized mainly by the P1 spike, which occurs at the onset of stimulus activity and is very distinctive (**Fig. 2.19, 2.21**) with the P2 spike sometimes but not always present (**Fig. 2.18**). The P2 spike, if present, tends to be an elevated level of activity compared to background levels (during the no-stimulus portions of the battery), but is generally not greater than DMSO activity (**Fig. 2.21, 2.22**). Referring back to the tSNE analysis (**Fig. 2.17**), category A compounds can be further split into “toxic” and “non-toxic” subgroups. However, because the B compounds likewise have varying levels of toxicity but are more closely grouped with each other rather than the toxic A compounds, this suggests that something beyond toxicity - most likely the P1 spike - separates the toxic A and B compounds.

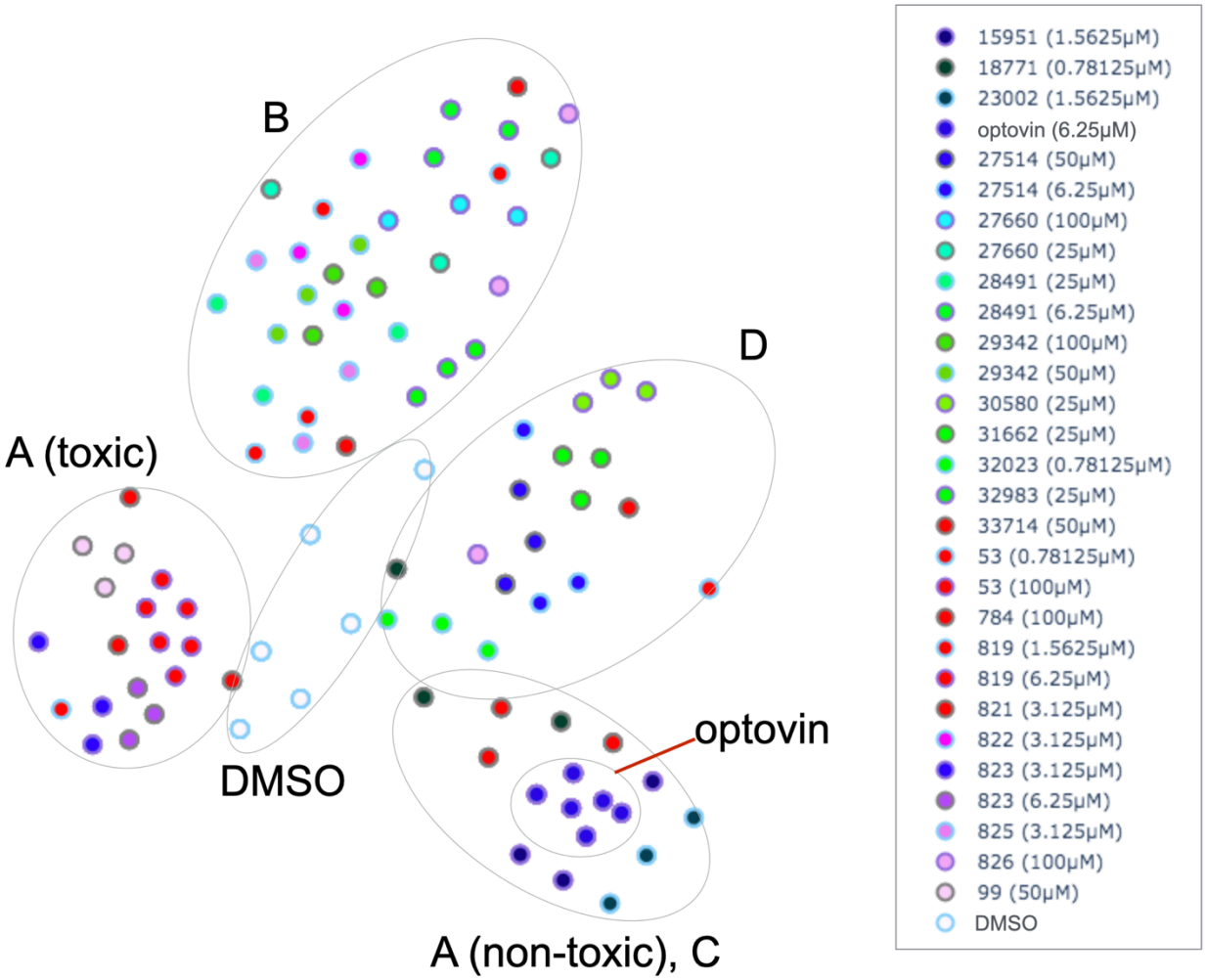

Figure 2.17 tSNE analysis of full activity traces reveals phenotypic clusters
tSNE analysis of full activity traces recorded from hit compound-treated larvae identifies clusters of compounds with similar phenotypes. Retroactive labelling following further analysis revealed that these groups closely correlated with the identified phenotypic clusters. n = 6 wells optovin, 6 wells DMSO, 3 wells per hit compound; 8 fish/well.

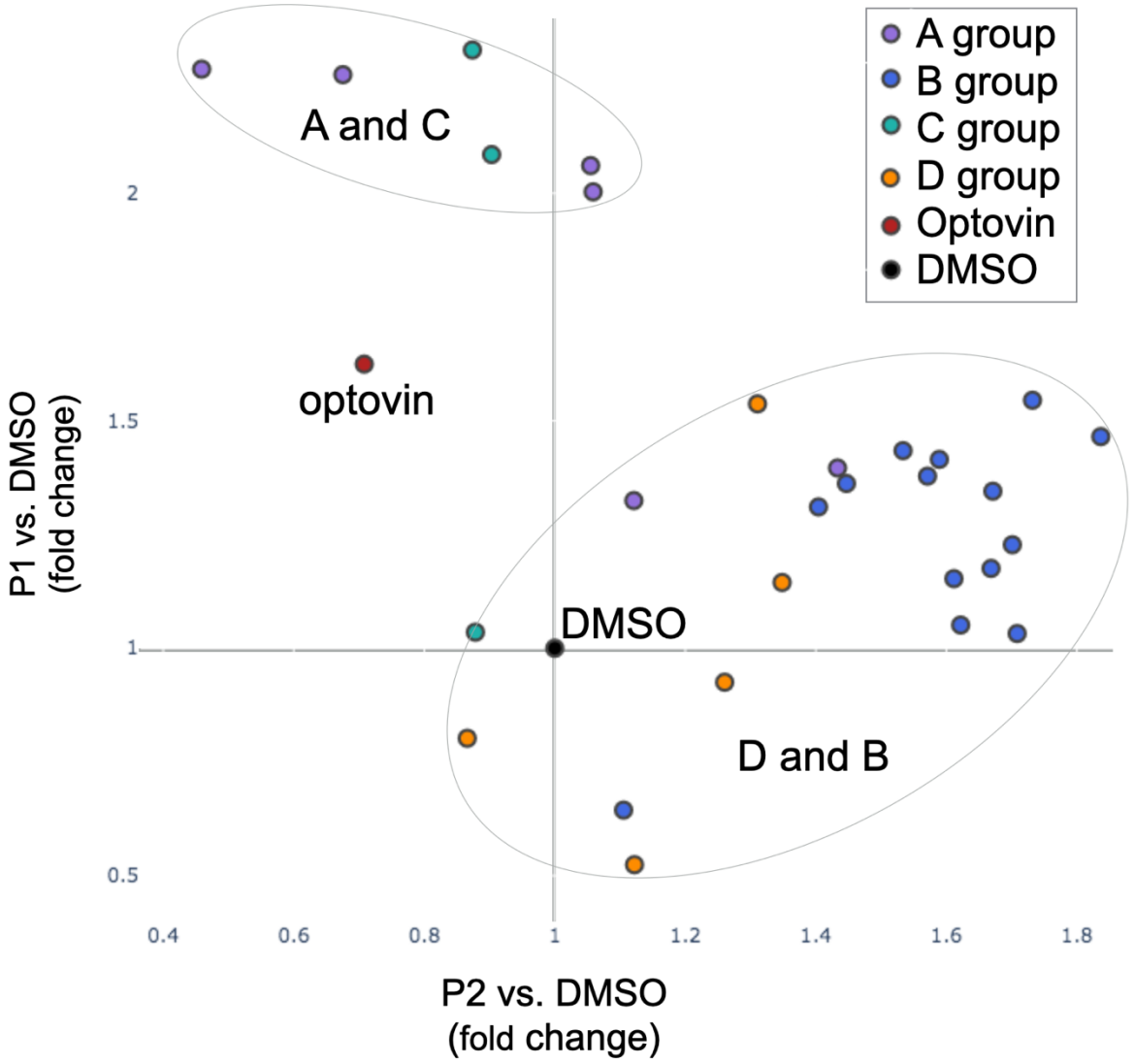

Figure 2.18 Pairwise scatter plot identifies behavioral phenotype signatures
Pairwise scatter plots identify the phenotypic features that best separate the groups identified in the tSNE analysis. Light responses for all compounds were first broken down into the optovin-defined phases (pre, P1, P2 and post, with P3 not represented in this test battery). Following pairwise comparisons, it was revealed that the P1 vs. DMSO and P2 vs. DMSO fold change measurements created the greatest separation between compounds. Retroactive labelling demonstrated that the presence of P1- or P2-like phases most strongly differentiated the A/C and B/D groups. n = 6 wells optovin, 6 wells DMSO, 3 wells per hit compound; 8 fish/well.

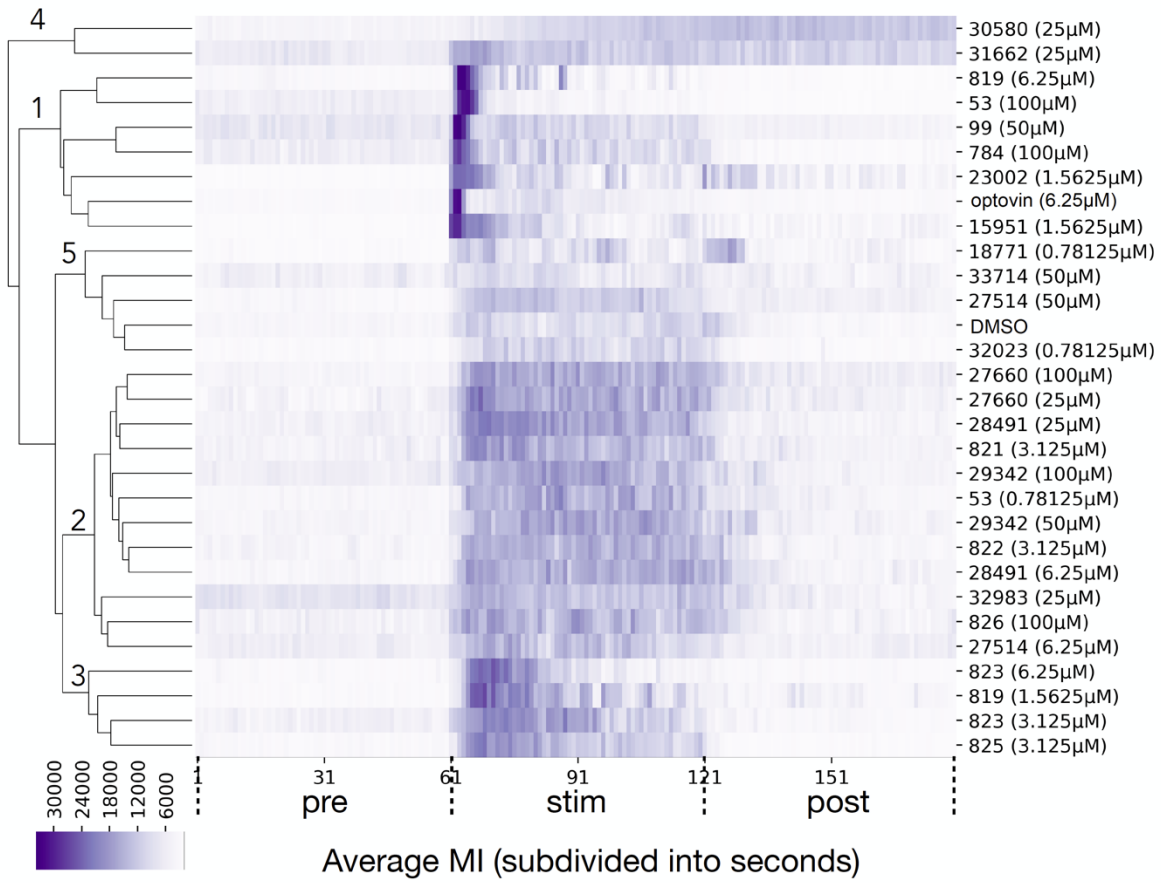

Figure 2.19 Heatmap analysis and clustering further define phenotypic groupings
As labeled, branch 1, which includes optovin, is defined by a very strong initial spike of activity in the first few seconds of the stimulus, while branch 2 is characterized by increased activity throughout the stimulus. The phenotype observed in branch 3 has characteristics of both 1 and 2. Branches 4 and 5 display more anomalous phenotypes, with branch 4 displaying an increase of activity beginning during the stimulus and continuing through the post-stimulus period, while activity in branch 5 shows little consistency. n = 6 wells optovin, 6 wells DMSO, 3 wells per hit compound; 8 fish/well.

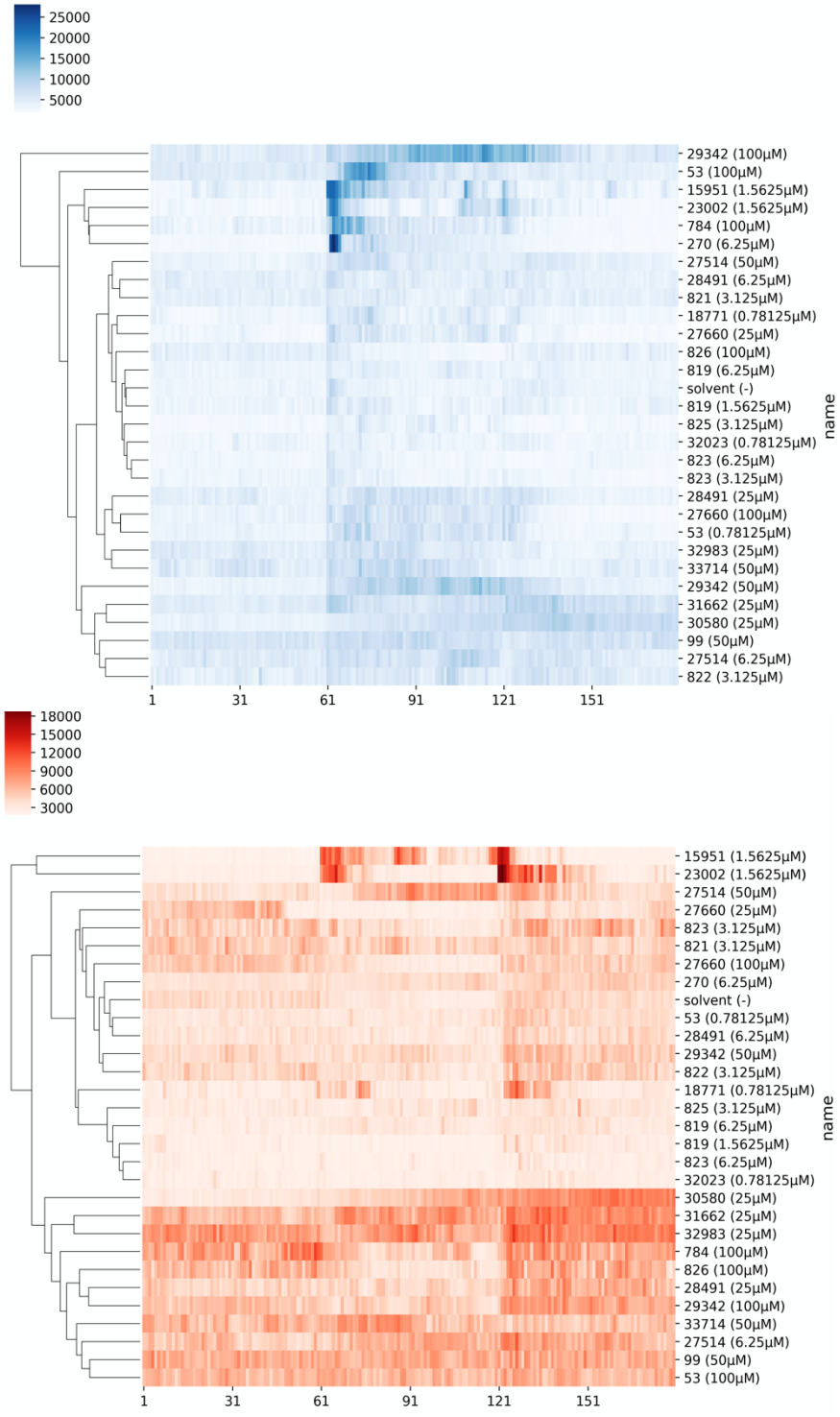

Figure 2.20 MI heatmap analysis and clustering for blue, red, and green wavelengths
Treated fish were exposed to either blue (460nm), red (660nm), or green (523nm) light. n = 6 wells optovin, 6 wells DMSO, 3 wells per hit compound; 8 fish/well. (cont'd on next page)

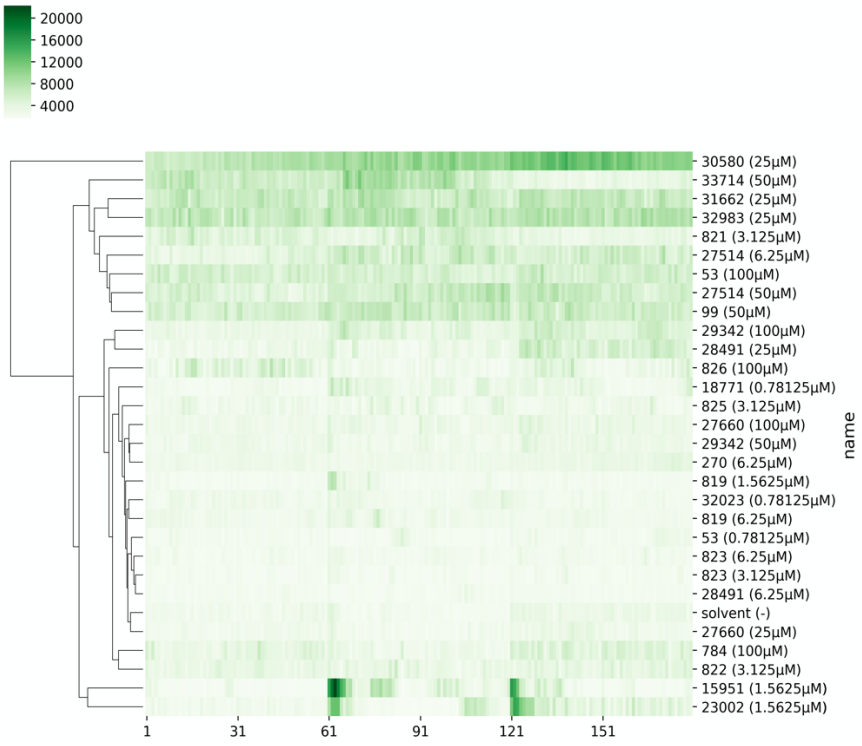

Figure 2.20 MI heatmap analysis and clustering for blue, red, and green wavelengths (cont'd)

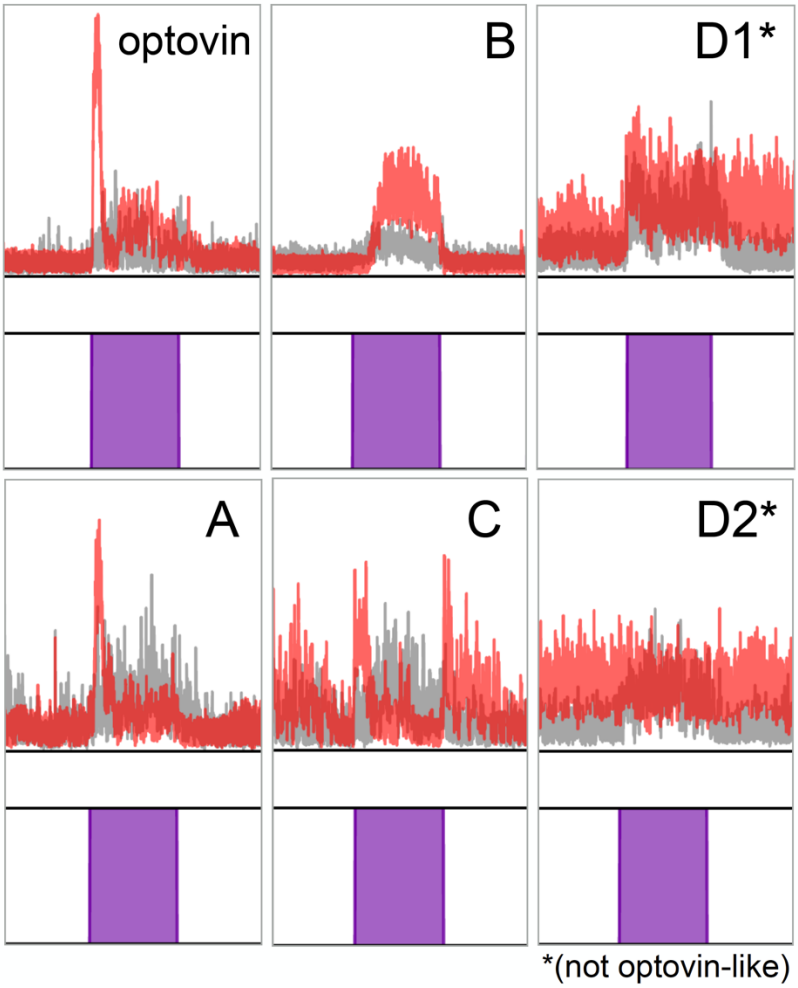

Figure 2.21 Representative MI traces for the four phenotypic subgroups
MI traces illustrate differences between the four behavioral phenotypes: A (most similar to optovin with a distinct P1 spike), B (purple light-sensitive with a P2-like response), C (on/off light responsive), and D (not optovin-like). Examples of each are shown here, including two examples for group D (red traces represent hit compounds, gray traces represent DMSO). Examples A, C, D1, D2: n = 3 wells; 5 fish/well. Examples for optovin, B: n = 3 wells; 8 fish/well.

Table 2.7 Classification of hit compounds for all wavelengths

Compound ID (dose, μM)	Violet	Blue	Green	Red
optovin	A	A		
53 (0.78125)	B	B		
53 (100)	A	A		
99 (50)	A			
784 (100)	A	A		
819 (1.5625)	A			
819 (6.25)	A			
821 (3.125)	B			
822 (3.125)	B			
823 (3.125)	B			
823 (6.25)	A			
825 (3.125)	B			
826 (100)	B			
15951 (1.5625)	C	C	C	C
18771 (0.78125)	C	C	C	C
23002 (1.5625)	C	C	C	C
27514 (6.25)	D	D	D	D
27514 (50)	D	D	D	D
27660 (25)	B	B		
27660 (100)	B	B		
28491 (6.25)	B			D
28491 (25)	B	D	D	D
29342 (50)	B	B		D
29342 (100)	B	B	D	D
30580 (25)	D	D	D	D
31662 (25)	D	A	D	D
32023 (0.78125)	B			
32983 (25)	B	B	D	D
33714 (50)	D	D	D	

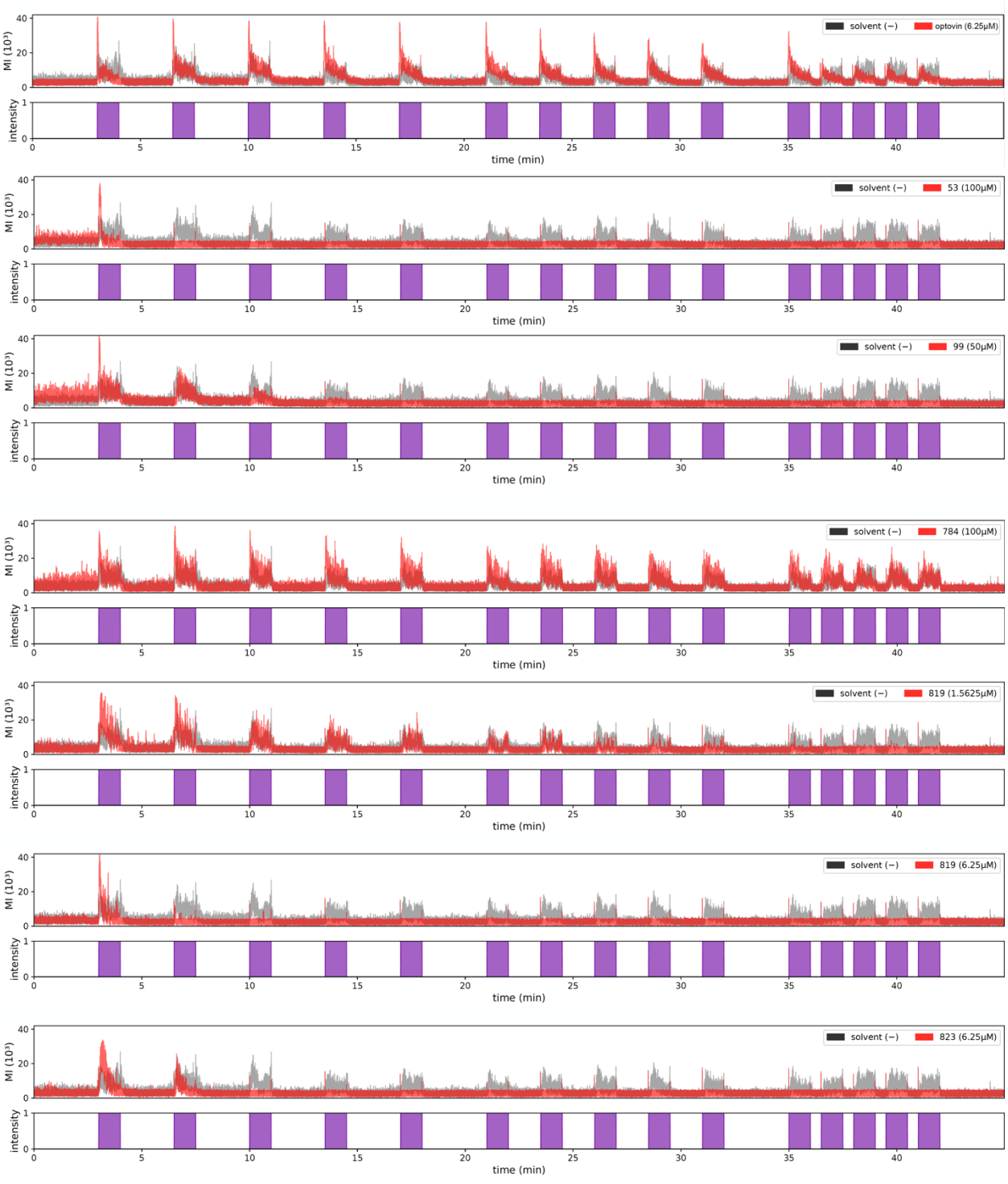

Figure 2.22 MI traces for A compounds.
The A compounds, including optovin, are characterized by a distinct spike of activity at the beginning of the stimulus. The P2 spike is sometimes but not always present.

The second group, Group B, included 13 compounds (**Fig. 2.21, 2.23, Table 2.7**). These compounds produced phenotypes that were characterized by large P2 spikes, the absence of P1 spikes (**Fig. 2.18, 2.21**), and consistently elevated activity while the stimulus is ongoing. This response is usually 1.5- to 2-fold higher than DMSO and continues for the duration of the 1 minute light stimulus. Notably, in contrast to the category A response, the first few seconds of the response (the P1 “spike” seen in category A) are not increased compared to the rest of the response (**Fig. 2.19, 2.21**). Similar to category A, post-stimulus response is approximately the same or below DMSO-induced response.

The third group, category C, included 3 compounds (**Table 2.7**) that displayed phenotypes very similar to those of optovin, but which can be distinguished by the presence of a second spike when the stimulus ends (**Fig. 2.19, 2.21, 2.24**). In this “on/off” (ONOFF) response, when the stimulus is first activated, a sharp spike of activity occurs, similar to the category A response. This similarity likely contributed to the inclusion of these compounds in the same clusters as category A compounds (**Fig. 2.17, 2.18, 2.19**). However, unlike the category A response, when the light stimulus is turned off, a second distinct activity spike is observed. Activity levels between the two spikes while the stimulus is ongoing are generally lower than DMSO, while post-stimulus activity is more variable than in both A and B, with occasional small spikes of activity. The three compounds that induce this behavior (15951, 18771, 23002) do so in response to all tested wavelengths of the light stimulus (**Fig. 2.19, 2.20, Table 2.7**).

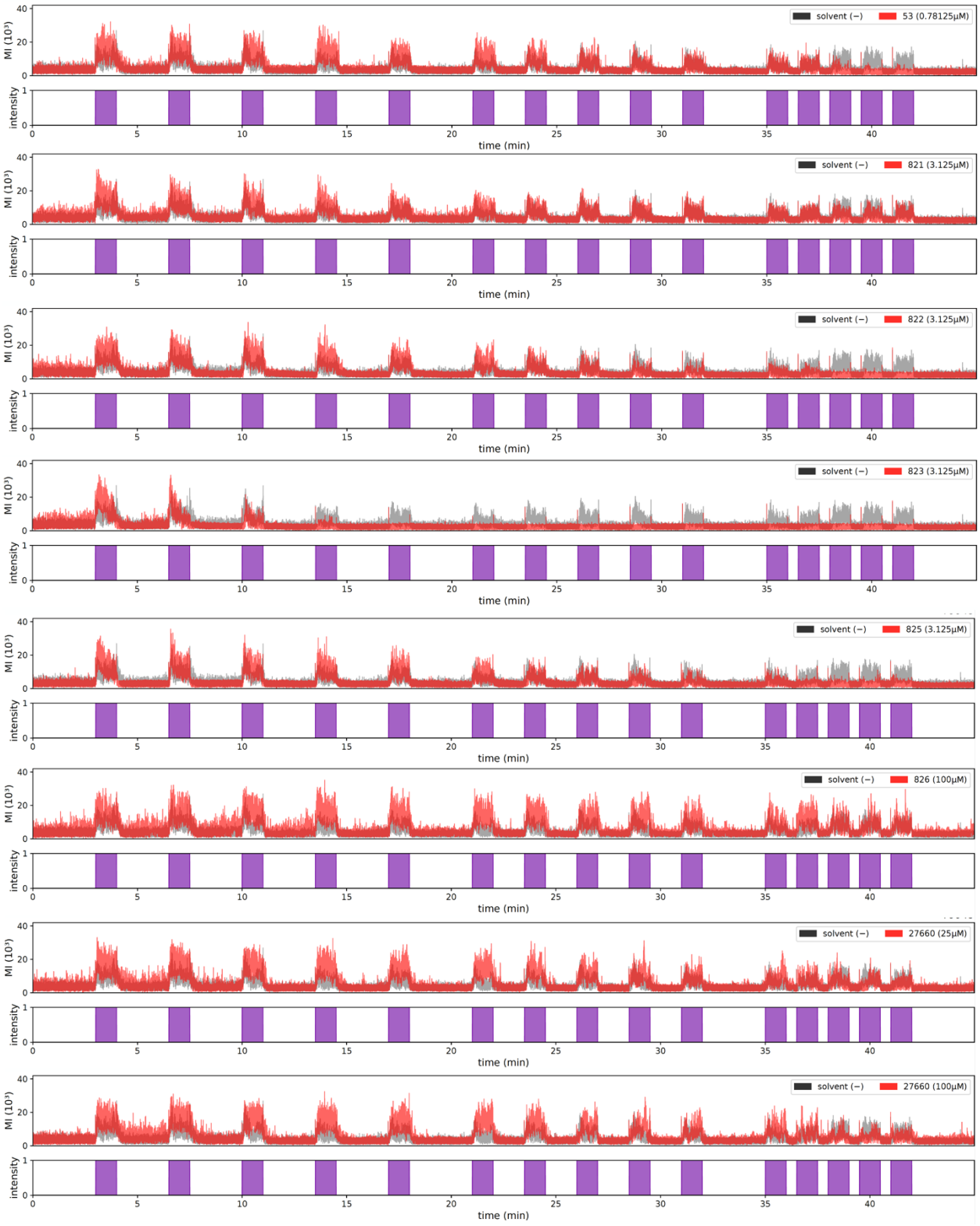

Figure 2.23 MI traces for B compounds
B group compounds are characterized by large P2 spikes and the absence of P1 spikes. Activity is consistently elevated while the stimulus is ongoing. (cont'd on next page)

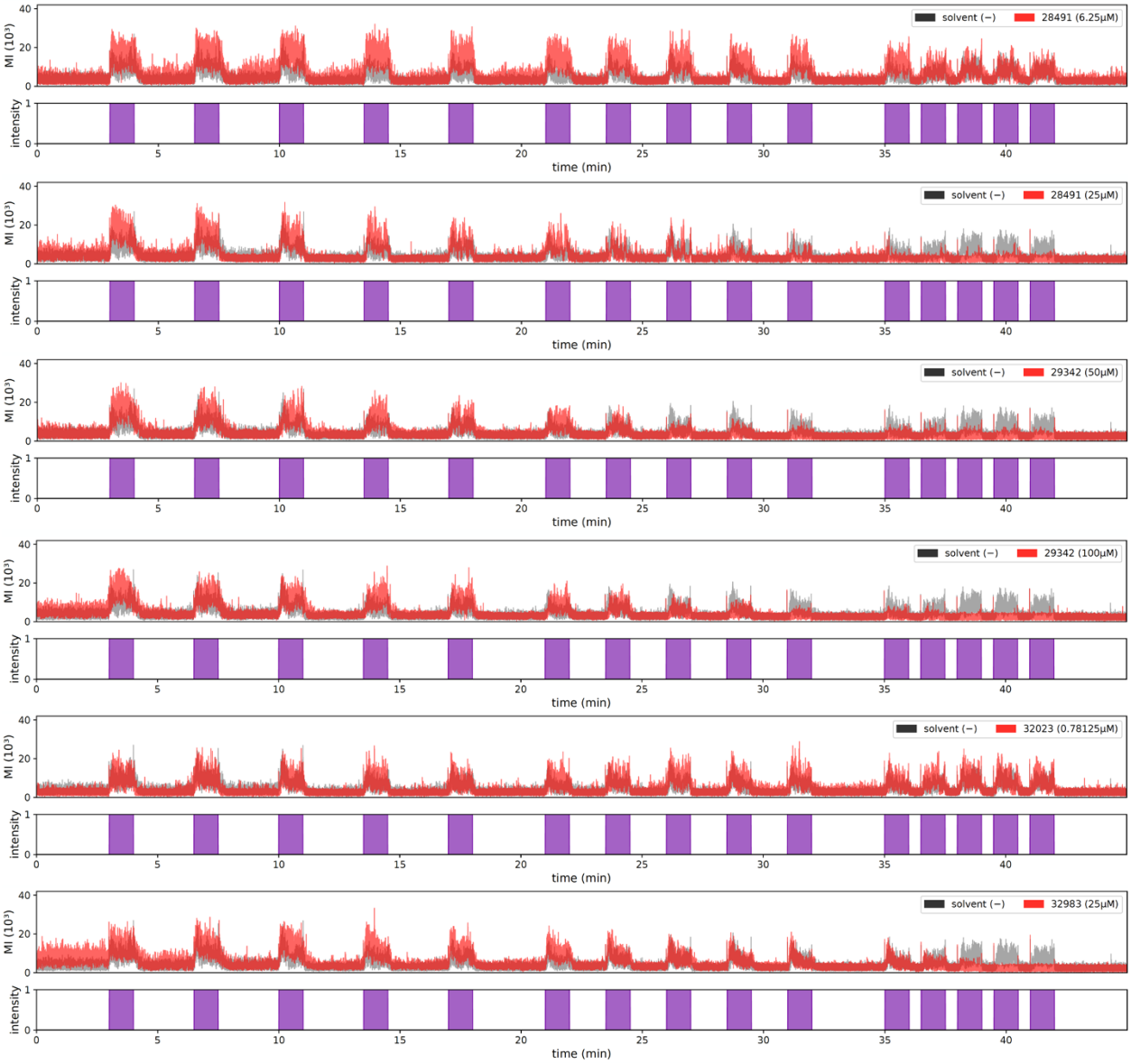

Figure 2.23 MI traces for B compounds (cont'd)

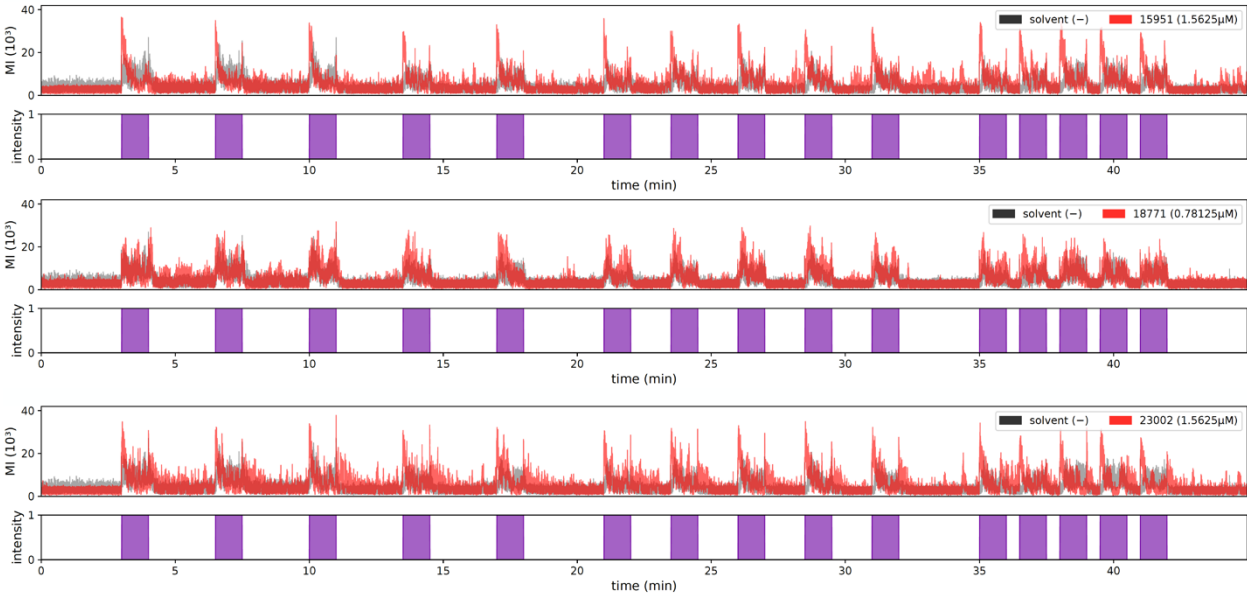

Figure 2.24 MI traces for C compounds
Group C compounds display a distinct “on/off” response. While the initial sharp spike of activity is very similar to that of the A group compounds, C group compounds also induce a second distinct activity spike when the light stimulus is turned off.

The fourth group, category D, included 4 compounds that generally increased overall motor activity (**Fig. 2.19, 2.21, 2.25**). While the responses in categories A, B, and C are to some extent optovin-like, category D consists of non-optovin-like light-dependent behaviors. In general, while these behaviors are affected by the light stimulus, the immediate response to a stimulus is only slightly higher than in controls, but the slight increase in activity continues even after the stimulus ends. Additionally, inter-stimulus activity levels tend to be more variable than in the first three phenotypic categories.

Interestingly, of the compounds tested, some compounds (53, 819) induced different types of activity at different doses, where at low doses the response was more similar to the B group compound response, and at higher doses the response was more similar to those induced by the A group (**Table 2.7, Fig. 2.22, 2.23**). Furthermore, both long- and short-term toxicity of these compounds is mixed (**Fig. 2.16**). In addition to violet light, blue, red, and green light stimuli were tested as well (**Fig. 2.20, Table 2.7**), revealing that similar patterns of behavior (A, B, C, or D) could be induced by these wavelengths, but not necessarily by the same compounds. For many compounds, blue light induced the same type of behavior in fish as violet light, but for others, blue light induced a different response or none at all (**Fig. 2.20, Table 2.7**). Red and green light in combination with hit compound treatments were less likely to elicit any response whatsoever, and those that did tended to induce category C or D behaviors (**Fig. 2.20, Table 2.7**).

Since the hit compounds cluster into distinct phenotypic subclasses, these data suggest that each subclass may represent a different biological mechanism. For example, one of the most distinct clusters, the compounds that produce the ONOFF phenotype, may depend on different molecular targets than either optovin or the other hit compounds.

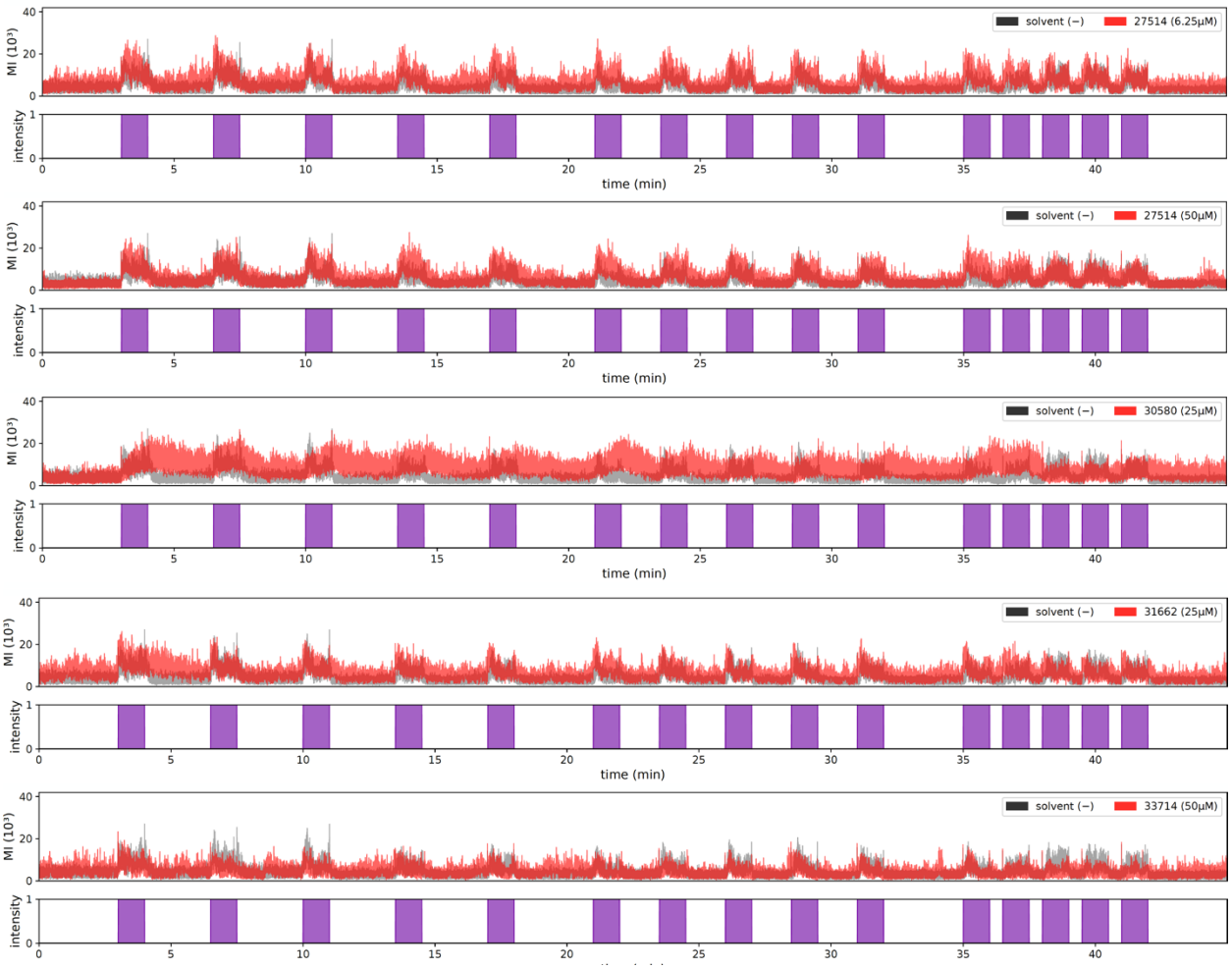

Figure 2.25 MI traces for D compounds
The D group consists of compounds that generally increase activity in a light-dependent but non-optovin-like manner. While these behaviors are affected by the light stimulus, the immediate response to a stimulus is only slightly higher than in controls, and the increase in activity continues even after the stimulus ends. Additionally, inter-stimulus activity levels tend to be more variable than in the other three phenotypic categories.

A subset of hit compounds act via TRPA1b

Previous studies have shown that optovin produces non-visual TRPA1-mediated photosensation[25]. However, it remains unclear if any of the novel hit compounds depend on either vision or TRPA1. To answer this question, we analyzed the effects of mutations affecting TRPA1b, as well as ATOH7, a gene that is required for the development of retinal ganglion cells and the loss of which results in complete blindness[35].

Group A and B compounds, which induced activity most similar to that of optovin, were generally found to be dependent on TRPA1b (**Fig. 2.26, 2.27**). Conversely, group C activity is dependent on ATOH7, but not TRPA1b (**Fig. 2.26, 2.27, 2.28**). Group D activity did not depend on TRPA1b, but the dependence of this group as a whole on ATOH7 is unclear (**Fig. 2.26, 2.27, 2.28**). From the A group, P1 spiking was abolished in the TRPA1b mutants for four out of the five hit compounds. The last compound likewise followed a similar trend, though the change in response did not reach significance **(Fig. 2.26, 2.27**). Similarly, the optovin response was abolished in TRPA1b mutants. Conversely, treatment using the A group compounds in ATOH7 KO fish did not result in a reduced response (**Fig. 2.28**). Similarly, in Group B, P2 spiking was also abolished in TRPA1 mutants for six out of eleven compounds, but not in ATOH7 or WT controls **(Fig. 2.26, 2.27, 2.28**). By contrast, for the two tested group C compounds, ONOFF was abolished in ATOH7 mutants. However, this did not occur in WT controls or in TRPA1 KOs, in which all three group C compounds were tested **(Fig. 2.26, 2.27, 2.28**). Finally, in Group D, no compounds induced a significantly different response in TRPA1bKO fish compared to the WT fish. Two group D compounds were tested in the ATOH7 fish; of these, one showed a significant decrease in response **(Fig. 2.26, 2.27, 2.28**). Together, these data suggest that compounds in Group A and B, like optovin, produce non-visual TRPA1-mediated photosensation. By contrast, the compounds in group C act on visual pathways.

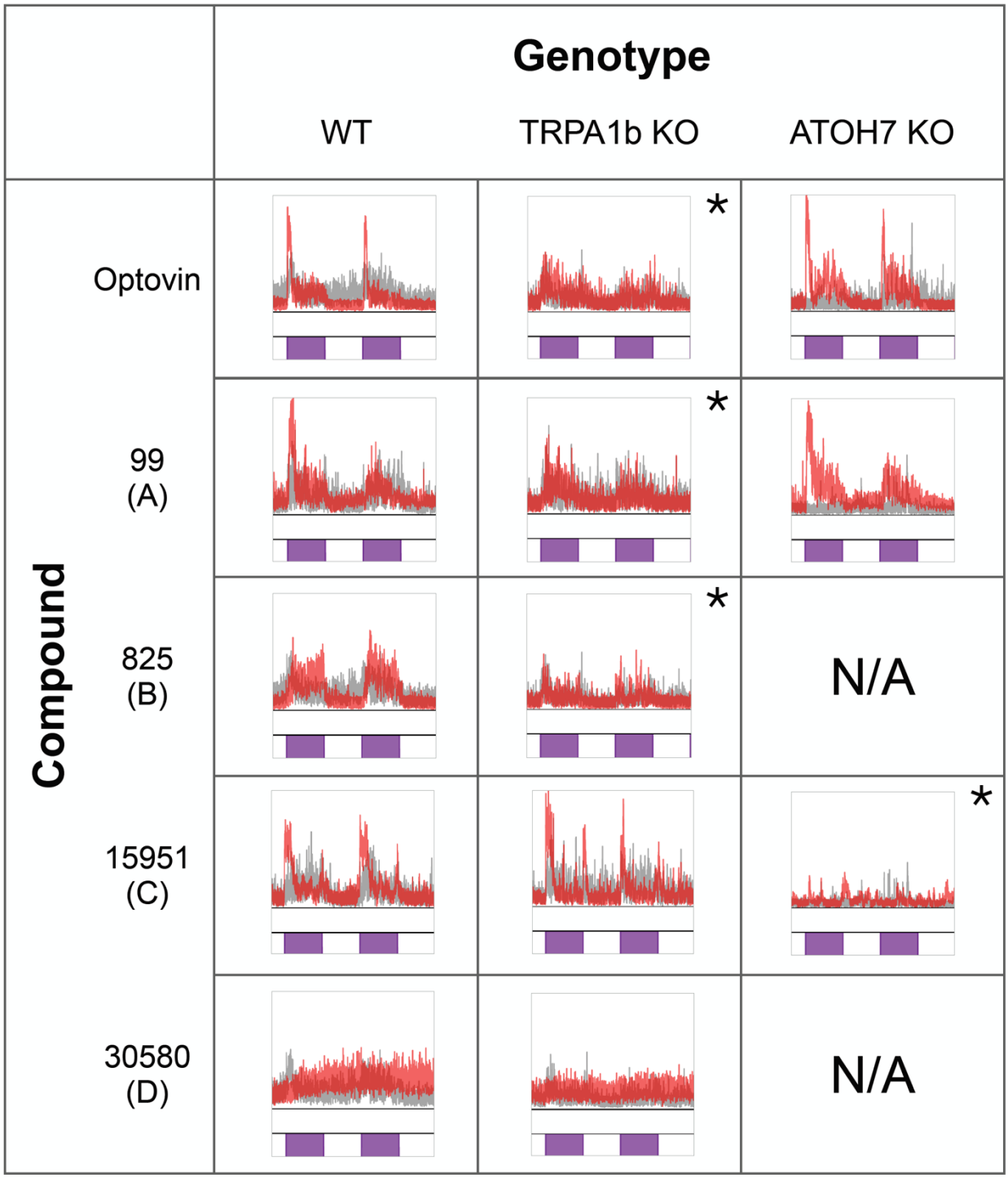

Figure 2.26 Example MI traces demonstrating TRPA1b or ATOH7 dependence
Example traces illustrate the effect of hit compounds from different phenotypic groups in WT, TRPA1b KO, and ATOH7 KO fish compared to background-matched controls. n = 3 wells; 5 fish/well. *p < 0.05.

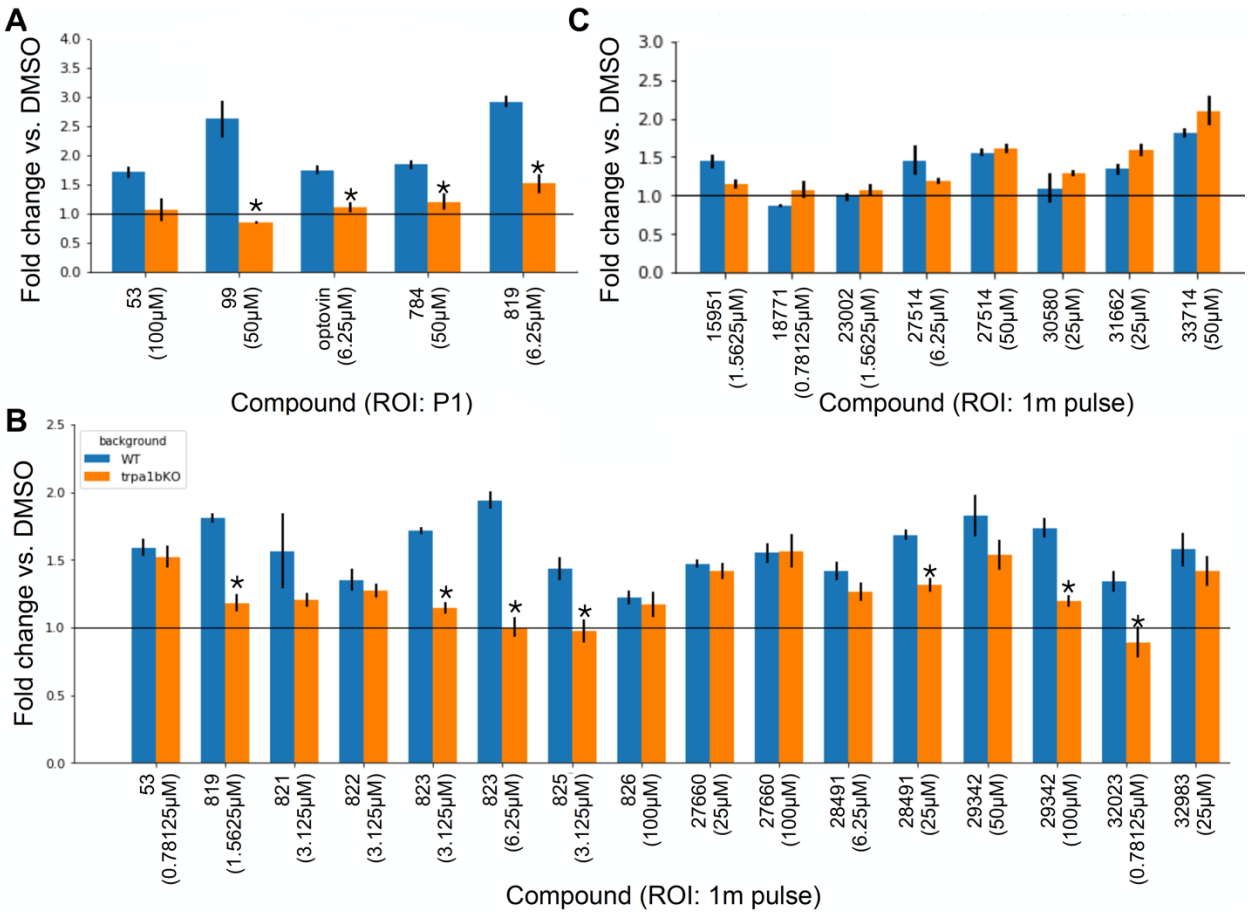

Figure 2.27 A subset of hit compounds act via the TRPA1b receptor

Bar plots depict the response fold change of WT and TRPA1b KO fish treated with hit compounds against DMSO-treated background-matched larvae. n= 14 wells per compound per genetic background for DMSO and optovin, 3 wells per compound per genetic background for hit compounds, 2 wells per compound per genetic background for no treatment; 5 fish/well. Error bars represent SEM. *p<0.05.

(A) A group compounds; response measured during P1 phase.

(B) B group compounds; response measured throughout the first stimulus (1 min).

(C) C/D group hit compounds; response measured throughout the first stimulus (1 min).

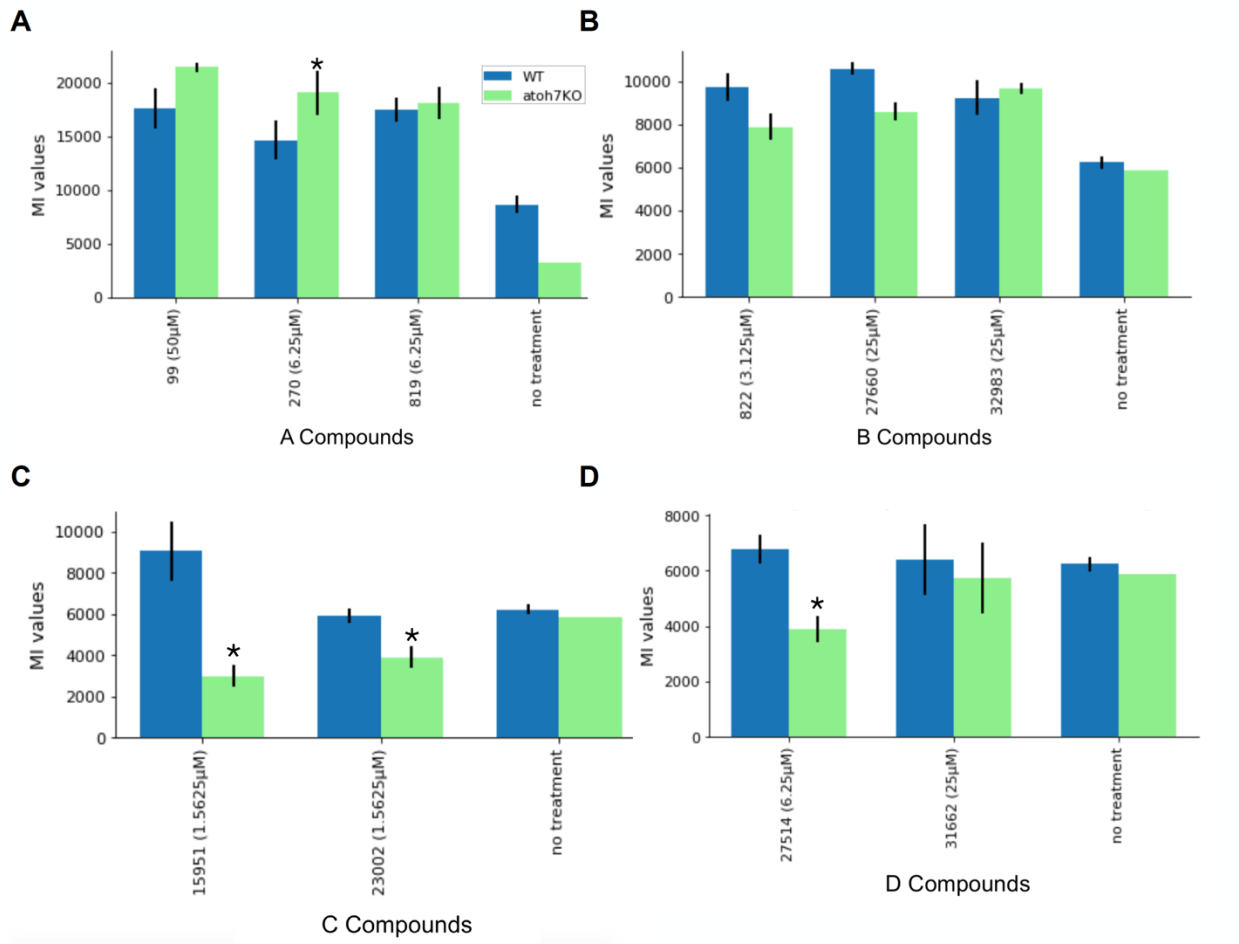

Figure 2.28 A subset of hit compounds requires ATOH7
Mutation of the *atoh7* gene in zebrafish results in the complete elimination of the retinal ganglion cells, rendering the fish blind. In order to determine whether the compound effects were vision-dependent, the hit compounds were tested in ATOH7 KO fish. n = 3 wells per compound per genetic background for hit compounds except 784, 6 wells per genetic background for 784, 8 WT and 7 ATOH7 KO wells for optovin and DMSO, 12 WT and 1 ATOH7KO wells for no treatment; 5 fish/well. Error bars represent SEM. *p<0.05.
(A) A group compounds; response measured during P1 phase.
(B-D) B, C, and D group compounds, respectively; response measured throughout the first stimulus.

DISCUSSION

We demonstrate here that a wide variety of structurally diverse novel compounds can produce non-visual photosensation via TRPA1 in zebrafish (**Fig. 2.29**). Evidence suggests that these compounds are photoreactive and depend on TRPA1b, and that they induce different patterns of behavioral phenotypes. These observations extend our understanding of the pharmacology of TRPA1-mediated non-visual photosensation beyond compounds structurally related to optovin.

Light responsive compounds demonstrate structural diversity

Although previous studies had identified optovin analogues[36], it was unclear whether TRPA1-mediated non-visual photosensation also occurred with other, more structurally diverse compounds. Through this study, we have demonstrated that there are multiple novel compounds with structural and photochemical properties that differ greatly from those of optovin, but yet are similarly able to induce motor activity in response to light. Previously, optovin's photoactive properties have been linked to its rhodanine ring. However, the majority of photoactivatable compounds identified here do not contain this moiety, suggesting that a rhodanine ring may not be required to confer TRPA1-mediated non-visual photosensation.

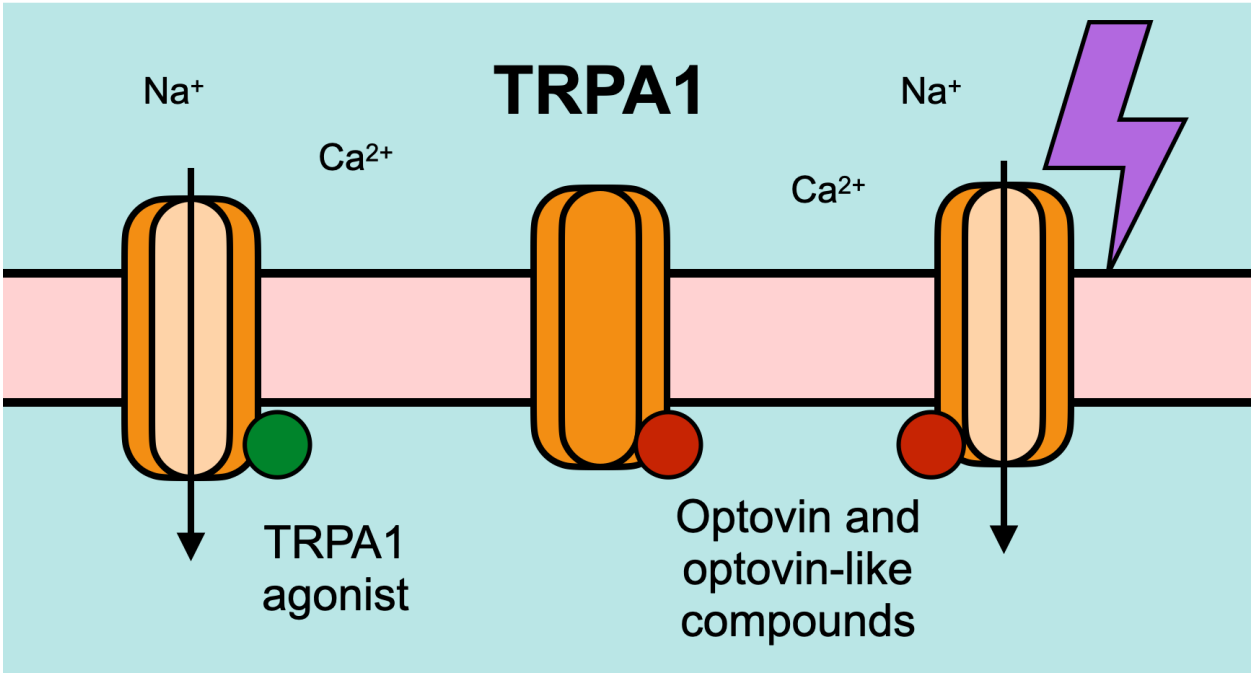

Figure 2.29 Novel compounds produce non-visual photosensation via TRPA1
For the majority of known TRPA1 agonists such as AITC or CA, binding to the allosteric nexus of TRPA1 will open the channel. However, for optovin and the novel optovin-like compounds identified in this screen, channel opening requires both binding and exposure to light, most commonly in the violet or blue wavelengths.

Hit compound phenotypes cluster into four distinct categories

Phenotypically, we observed that the compound responses to violet light tended to cluster into four main categories. Groups A and B comprised compounds that induce optovin-like phenotypes, with A defined by an initial sharp spike of activity (equivalent to P1 in optovin) and B defined by a more gradual increase in activity (equivalent to P2). This split was unexpected, as we initially believed that all optovin-like compounds would have a similar behavioral profile. One potential explanation for this is that the hit compounds - or, possibly, their light-activated configuration - may have varying affinities for TRPA1. Compounds with higher affinities would bind to and activate more channels, thus rapidly inducing a large amount of activity via the receptor, while compounds with lower affinities would not bind as frequently, resulting in fewer channel openings and therefore slower, more sustained activity that does not reach as high of a magnitude. Likewise, compound availability may be a limiting factor in receptor binding and may be affected by blood protein binding[37] or distribution into the tissues[38], or, if the compounds are acting on TRPA1 receptors in the brain, slow or limited passage across the blood-brain barrier[39]. This is supported by the observation that several of the compounds tested at multiple doses (53, 823) switch from B-type activity at the lower dose to A-type activity at the higher, where an increased dose would result in more of the compound being available to bind to receptors[40]. However, other compounds did not display A-type activity at any tested dose. In these cases, a possible explanation for B-type activity is that while the compounds may be readily available in their inactive state, they may undergo a slower conversion to the light-activated binding form, thus accounting for the relatively slower increase to maximum activity levels observed with B compounds.

Conversely, group C and D compounds did not induce optovin-like phenotypes. Group C compounds, despite their similarity to the A group due to the initial P1-like spike of the phenotype, also induced a secondary, smaller spike when the stimulus turned off,

demonstrating a novel mode of light response. Group D consisted of compounds that induced phenotypes that were not similar to optovin and did not fit with the other categories. However, as these groups were not shown to act via TRPA1, it is difficult to speculate on their mechanisms.

Optovin-like compounds demonstrate the greatest response to blue and violet wavelengths

In order to determine whether the light-induced phenotypes were specific only to violet light, we also tested the response to blue, red, and green wavelengths and categorized them using the same groups as for the violet-light response. In accordance with the observation that optovin also demonstrates a strong response to blue light, many of the A and B group compounds likewise respond to blue light stimuli, and for each compound the blue light activity type resembles that of the violet light. Considering all light dependent activity, we observed fewer responses to green and red wavelengths. This is in line with previous research[41], as light in these wavelengths carry less energy than light in blue or violet, and therefore would possess less energy to contribute to structural changes. Because of this, it would be useful to perform a screen based on blue light activity to further probe the relationship between compound, wavelength, and receptor, and to identify whether blue light sensitivity exists independent of violet light sensitivity.

Interestingly, we observed that C and D compounds demonstrated activity in response to all four wavelengths. This suggests that both the responses of C compounds, whose activity is clearly light-dependent, and most D type compounds, whose activity is more generally unspecific, are more of a generalized, non-wavelength-specific light response.

Finally, we also noted that several compounds responded differently to the four wavelengths; for example, compound 32983 showed B type activity in blue and violet, but D type activity in red and green. For compounds shown to require TRPA1b (28491, 29342), it is possible that these may have off-target effects that are either suppressed during blue/violet stimuli or that are activated only in response to green/red light. For other compounds that are not TRPA1b dependent (31662), or whose TRPA1b status is unclear (32983), their activity may be due to a completely different receptor whose light-dependent activity has yet to be identified, or the activity may in fact be TRPA1b dependent, but in wavelengths other than violet. While in depth testing of responses to all wavelengths was beyond the scope of this study, this represents an intriguing direction for understanding the role different wavelengths play in light-dependent, small-molecule-induced behaviors.

Absorbance and fluorescence of hit compounds varies greatly

In addition to their structural and phenotypic features, we also investigated several photochemical properties of these compounds to determine if there were features that were common to all light-activated compounds. Though the wavelength at which absorbance occurred varied, optovin and all A and B group compounds exhibited some degree of absorbance. C and D compounds, however, did not demonstrate any absorbance. Together, this suggests that absorbance is required for light-dependent activation of TRPA1.

Prior exposure to violet light (for time periods ranging from 5 to 1200 seconds) had either no effect or reduced absorption on most hit compounds and optovin, which was expected due to the possibility of bleaching or non-reversible light-dependent structural changes. Interestingly, in some compounds (28491, 29342, 31662), prior exposure in fact greatly increased absorption, suggesting that the addition of light energy induced structural changes that increased the likelihood of energy absorption. The degree by which absorption changed did not seem to

correlate to baseline absorbance (t0). Some compounds that demonstrated baseline absorbance showed very little change, while some compounds that did not (C group, 27514, 31662) were affected by multiple exposures to light, with one (31662) surprisingly showing a very large increase. Generally, the wavelengths at which peak absorbance occurred were most affected by multiple irradiation, but this was not always the case. It remains unclear if changes in absorption, whether increasing or decreasing, are linked to the identified behavioral phenotype groups; for example, whether an increase in absorption resulting from prior violet light exposure would allow compounds not in groups A or B to induce A- or B-type activity.

Finally, the majority of hit compounds and optovin, as well as the DMSO control, did not demonstrate notable maximum excitation or emission wavelengths (**Table 2.4**). Interestingly, outlier compounds were all found to be in either Group A or Group B. This suggests that there may be two different mechanisms behind the optovin-like response - one that involves photoreactivity, and one that occurs in the absence of it. For the Group C and Group D compounds, however, photoreactivity does not seem to be important.

Phototoxicity is wavelength dependent

Surprisingly, we noticed that exposure to violet and blue wavelengths significantly increased toxicity in many instances. Following the development of an experiment to test if light wavelength had an effect on compound toxicity, we found that this was indeed the case for many compounds following violet and blue light exposure, suggesting that these compounds are inert or mostly inert until activation by specific wavelengths. No compounds demonstrated significant increased toxicity following exposure to green or red wavelengths (compared to the no stimulus control), and baseline toxicity was observed in only two compounds (increased toxicity in the no stimulus control compared to the no stimulus DMSO control). Intriguingly, in one compound that displayed baseline toxicity (30580), exposure to red light actually increased

survival time, suggesting a protective effect that warrants further investigation in future studies. Based on these experiments, we believe that the energy provided by violet or blue light is necessary for the conversion of these compounds to their active form, which then allows them to bind to receptors and induce an effect. Potentially, when these receptors are continually activated for long periods of time, their effect eventually becomes toxic. As many of the compounds that demonstrated increased toxicity were shown to be TRPA1b dependent, it is therefore possible that this receptor is TRPA1b. Future iterations of these experiments utilizing TRPA1bKO fish will help to confirm this and to determine the mechanism of toxicity.

Optovin-like hits are TRPA1b dependent

In this study, TRPA1b dependence was observed in many of the A and B compounds, but not in any of the C and D compounds. To confirm TRPA1-dependence, we developed a line of TRPA1b KO zebrafish and assessed if their activity matched that of wild-type fish following treatment and stimuli exposure. Additionally, to determine if any of the induced behaviors were vision-dependent, we obtained zebrafish with a mutation in *atoh7*, which causes the complete loss of retinal ganglion cells and results in completely blind fish. Of the 14 A and B group compounds, 8 demonstrated a significant loss of phenotype in the TRPA1b KO fish, with several others approaching significance. However, of the A and B group compounds tested in ATOH7 KO fish, loss of vision did not have an effect on this behavior. Conversely, TRPA1b dependence was not observed in any of the C and D compounds. However, of the compounds tested, loss of vision resulted in loss of the phenotypes induced by three compounds in this group (C: 15951, 23002; D: 27514). Taken together, these results indicate that while some compound induced behaviors, especially those most similar to optovin-induced behaviors, are non-visual and are mediated by TRPA1b photosensation, others are acting through different receptors and mechanisms. Of these, the C type compounds are of special interest; while they share with

optovin the ability to induce light activated behaviors, they differ greatly in phenotype, wavelength response, vision dependence, and target.

However, one potential constraint should be noted while interpreting this data. Due to the limited availability of mutant fish, genetic experiments were limited to 5 fish/well instead of the usual eight, which has previously been demonstrated to produce the strongest results when using our automated behavioral phenotyping system[42]. Consequently, more subtle phenotypes and any differences in WT versus mutant fish may have been suppressed, especially from compounds tested at lower doses. Additionally, only a selected subset of compounds from each phenotypic group could be tested in the ATOH7 KO fish. Because of this, while certain trends can be observed, it is difficult to draw conclusions about the role of ATOH7 in each hit compound group. Further studies utilizing 8 fish/well and additional replicates will be important for a comprehensive understanding of the targets of these hit compounds, and will continue once activity restrictions resulting from the COVID-19 pandemic have been lifted.

Future directions

While this study has revealed that a wide diversity of structures, photochemical properties, behaviors, and toxicities exist among light-dependent TRPA1 agonists, further research is needed to better understand both the mechanisms and the research or therapeutic potential of these compounds. Further structural analyses would help to elucidate the chemical moieties and energy changes responsible for light activation, allowing for the development of purpose-build analogues. Likewise, a better understanding of receptor-compound kinetics and the mechanisms of the hit compounds would help to answer questions about where and how the compound is binding, whether light activation occurs at the receptor-compound complex or on the compound alone, and whether any intermediates or downstream signaling pathways of TRPA1 play a role in the induced behaviors. To this end, patch clamp experiments could help to

reveal patterns of channel opening and the location of binding, while mutations in potential TRPA1 binding sites could confirm those locations[43]. The presence of intermediates such as reactive oxygen species (ROS) could be detected by co-treating with DABCO, a ROS quencher, or by using a singlet oxygen indicator dye such as singlet oxygen green[41], while bleaching or "pre-activation" of compounds would help to determine if exposure of only the compound to light is sufficient to induce the observed phenotypes. To ascertain the activity of these hit compounds on an organism-wide level, experiments on headless fish (as described in Kokel et al. 2013[41]) could identify whether the compounds act in the brain or in the periphery, and if in the brain, pERK imaging could identify the specific location, while mass spectrometry analysis could reveal the neurotransmitters affected. Finally, it is crucial to determine whether these results carry over into other species. Mouse studies would reveal the effect of these compounds in a mammalian model, and comparisons to the effects of known TRPA1 agonists such as AITC could reveal key differences in their action. Furthermore, experiments on human TRPA1 transfected cells would confirm the compounds' ability to induce an effect in humans, and thereby open the door for potential medical research or therapeutic use.

METHODS

Fish maintenance, breeding, and compound treatments

Eggs (up to 10,000 per day) were collected from group matings of wild-type "Singapore" zebrafish, and raised until 7dpf on a 14/10-hour light/dark cycle at 28^{o}C in egg water (60 µg/ml "Instant Ocean" Sea Salts in distilled water, then buffered and brought to a pH of 7.0-7.4 using sodium bicarbonate[44]). Following sorting for healthy zebrafish and temporary anesthetization using egg water chilled to 4^{o}C, eight larvae (as described in McCarroll et al. 2019[28]) and 300µL of egg water per well were distributed into square 96-well plates (GE Healthcare Life Sciences) using a p1000 pipette. Plates were allowed to return to room temperature over 1 hour, after

which compounds diluted in DMSO were applied directly to the egg water. Larvae were incubated following treatment for an additional hour before behavioral analysis. All zebrafish procedures were approved by the UCSF's Institutional Animal Care Use Committee (IACUC) in accordance with the Guide to Care and Use of Laboratory Animals (National Institutes of Health 1996) and conducted according to established protocols that complied with ethical regulations for animal testing and research.

Compound preparation and chemical libraries

Chemical libraries were selected and purchased from the Chembridge DIVERSet Screening Libraries. All chemical library compounds were stored at -80C and dissolved in DMSO, then further diluted in DMSO and screened at a final concentration of 10μM in <1% DMSO. All controls were treated with an equal volume of DMSO. Hit compounds were obtained from commercial sources (Hit2Lead, TimTec, Molport, Vitas, Mcule, ChemDiv). Optovin was obtained from Tocris (4901), DMSO from Sigma Aldrich, AITC from Sigma Aldrich (36682-1G), and cinnamaldehyde from Sigma Aldrich. Following receipt, compounds were initially diluted to 30mM stock solutions in DMSO and stored at -20^{o}C. Immediately prior to treatment, compounds were thawed at room temperature and further diluted with DMSO as required.

Automated behavioral phenotyping assays

Phenotypes were induced and recorded using a custom-built instrument that includes a camera, lighting, and various light, audio, and physical stimuli, as described in Myers-Turnbull et al. 2020[42] and McCarroll et al. 2019[28]. Briefly, plates were placed in the instrument on a custom build acrylic stage and illuminated with a 760nm infrared light, and an AVT Pike digital camera (Allied Vision) fitted with an infrared-passing/visible light-blocking filter (LEE Filters LE8744 polyester #87) and mounted to a telecentric lens captured images at 25fps. Light stimuli were delivered using high-intensity LEDs and included red at 623nm (1537-1041-ND, DigiKey), green

at 525nm (1537-1039-ND, DigiKey), blue at 460nm (1537-1037-ND, DigiKey), and violet at 400nm (LZ4-40UB00-00U7, Mouser). Acoustic stimuli were delivered using a computer to playback audio stimuli as MP3s using an APA150 150W powered amplifier (Dayton Audio) played through surface transducers adhered to the acrylic stage. Physical tapping stimuli were delivered using push-style solenoids (12V) to tap the stage. Instrument control, including data acquisition and stimulus activation, was conducted using custom MATLAB and Python scripts. Processing of video data to the zebrafish motion index (MI) was calculated as follows:

$MI = \text{sum}(\text{abs}(\text{frame}_n - \text{frame}_{n-1}))$.

Optovin and TRPA1b agonist activity analysis

Optovin phases were identified from data collected during a single, 10 minute long purple stimulus. Phases were defined as follows: Pre-stimulus ("pre") begins at the start of the battery and ends at stimulus start. The average of this phase is also the optovin baseline. Phase 1 ("P1") begins at stimulus start and ends following the occurrence of the lowest MI within the first 30s of response. Phase 2 ("P2") begins following P1 and ends following the occurrence of the first MI value that is less than or equal to the optovin baseline. Phase 3 ("P3") begins following P2 and continues through the end of the stimulus. Post-stimulus ("post") begins following the end of the stimulus and continues through the end of the battery. Average MI values are averages throughout each phase for each individual well, which are then averaged across all wells. Overall optovin activity in response to different stimulus wavelengths is shown as AUC, calculated as the sum of all MI values during the sixth one minute stimulus for each well, then averaged over all replicate wells. Optovin activity in comparison to known TRPA1 agonists is displayed as fold change vs. DMSO for each phase. Phases for all conditions are defined by optovin activity (as above), and values calculated by averaging MI over each phase for each well, then averaging data across all wells. Fold change was calculated by dividing each of these

values by the average DMSO value. Significance was calculated vs. optovin using Welch's t-test.

Compound screen hit identification and hit retest analysis

To identify first-level hits from screened library compounds, "regions of interest" (ROIs) containing violet wavelength stimulus were identified for each assay within the full battery. Average MI values from each ROI were then obtained for all compounds. Fold change vs. DMSO was then calculated by dividing values from each ROI for each compound by the averaged data from the equivalent DMSO control ROI from the same plate. A fold change value for each DMSO well was calculated in the same way, with ROIs from each DMSO on a plate divided by averaged data from the equivalent ROI for all other DMSO controls from the same plate. The maximum fold change value from each compound and DMSO was then selected and plotted as a histogram. Compounds that had a maximum fold change greater than +3σ from the mean were selected for further analysis. Following initial identification, hits were further filtered by several levels of analyses. Manual analysis of compound screen MI traces and video removed any anomalous traces, after which retesting at 10μM against the screening battery with three replicates identified compounds with reproducible phenotypes. Compounds that reproduced were then selected for dose-response testing at 8 doses between 0.78125μM and 100μM (x6 replicates) against the screening battery. ROIs were again selected and average MI values calculated. Significance for ROIs from each compound was calculated vs. same-plate DMSO wells using Welch's t-test. A dummy DMSO significance value was obtained by randomly splitting DMSO replicates from each plate into the "test" and "control" groups. The significance threshold was determined after applying the Bonferroni correction (0.05/3014 tests).

Photochemical analysis

Hit compounds and optovin were diluted to 100μM in egg water. An equal volume of DMSO in egg water and plain egg water were used as controls. To measure excitation/emission wavelengths, a 3D Fluorescence Scan was performed on a Tecan Spark. Compounds were plated onto a Grenier 384 well plate (Sigma, M6811). Emissions were measured every 20nm from 375-735nm, and excitations were measured every 20nm from 350-690nm. To measure absorbance, an Absorbance Spectrum experiment was performed on a SpectraMax M5 Microplate Reader (Molecular Devices). Compounds were plated onto a 384 well UV Star plate (Grenier Bio-One, 781801). Absorbance wavelengths were measured every 20nm from 250-750nm at 25C. For the multiple irradiation experiments, compounds were plated, then placed into the custom phenotyping instrument with the violet light stimulus activated. Immediately after light exposure, absorbance was measured as described above. Compounds were exposed to the violet light for varying lengths of time between 5 and 1200s and were freshly plated for each exposure.

Phototoxicity assay

Fish were incubated with hit compounds for 1 hour prior to stimulus exposure. After incubation, fish were placed into the behavioral phenotyping instrument and their activity tracked for 12 hours. During the first six, larvae were exposed to a light stimulus at one wavelength (blue (460nm), violet (395nm), red (660nm), green (523nm), or no stimulus), after which activity was tracked for an additional six hours. Time of death was determined by identifying the 5 minute window in which the standard deviation of activity (as measured by MI) was equal to or less than the overall standard deviation of activity in the 300μM eugenol-treated positive controls. Additionally, the standard deviation of the remainder of the MI trace (beginning after the 5 minute window) could not exceed the eugenol standard deviation; if it did, the next 5 minute window was selected and tested as above. Wells that did not meet these criteria within the 12

hour period were considered to have survived. Average length of survival was calculated by averaging time of death across all wells treated with the same compound and exposed to the same stimulus. Significance was calculated using Welch's t-test. For the violet, blue, red, and green conditions, the same compound with no stimulus exposure was used as the control. For the no stimulus condition, DMSO with no stimulus exposure was used as the control. A p-value of 0 indicates no difference from the control.

Structural and phenotypic clustering

Structural clustering was performed with custom Python scripts using the SciPy hierarchical clustering (fcluster, linkage) and distance (pdist, parameters: metric = 'jaccard') functions. Phenotypic tSNE analysis was performed on full MI traces with custom Python scripts using the scikit-learn tSNE function (parameters: perplexity=10, learning_rate=500, n_iter=3000, n_iter_without_progress=500). Pairwise comparisons of selected features were performed by first selecting features of interest and calculating the relevant values for each compound, including phases "pre", P1, P2, and "post" (individually) vs. DMSO fold change, P1 and P2 (individually) vs. baseline fold change, and average MIs for each individual phase. Each of these values was then plotted in a pairwise fashion and analyzed manually to identify the features that generated the greatest separation. Heatmaps were plotted by averaging MI values by second and using the Seaborn clustermap function. Final phenotypic classifications were determined manually. Following classification, phenotypic groups were retroactively labelled on the tSNE analysis and pairwise feature comparison to verify that manual classification was in agreement with quantitative clustering.

TRPA1b KO and ATOH7 KO zebrafish line development

The TRPA1b KO zebrafish line was generated using CRISPR to target a sequence (5' CTGCACTATGCTTCAGCTGG 3') in exon 3 of the *trpa1b* gene. Injections were performed as

described in Burger et al. 2016[45]. The F0 generation was allowed to mature into adults, then crossed with WT TUAB zebrafish. The resulting F1 generation was checked for the presence of a mutation using PCR and restriction digest with PvuII. DNA from fish with a mutation was then sequenced to confirm that the mutation introduced a stop codon, and F1s that had the same mutation were incrossed. From the F2 generation, TRPA1b -/- fish were selected and crossed, resulting in an F3 generation consisting entirely of TRPA1b -/- fish. To obtain larvae for experiments, F2 or F3 TRPA1b -/- fish were placed in breeding tanks with males and females separated the night before crossing. The next morning, the divider was pulled and any resulting embryos were collected. Larvae were used for behavioral experiments at 7dpf. ATOH7 (Lakritz) zebrafish larvae were generously provided by the Schoppik lab at NYU. Once the larvae were mature, fish were genotyped using PCR and restriction digest with StuI, and ATOH7 +/- fish were incrossed. ATOH7-/- larvae, which are visibly darker than ATOH+/+ or +/- fish, were then selected and raised. Because ATOH7-/- zebrafish are blind, it is necessary for them to be raised separately from homozygous or heterozygous fish to prevent outcompetition for food, and it is critical that for the first two weeks, the fish are provided with a high density of live food. To this end, starting at 5dpf, ATOH7-/- fish were raised in a separate tank and provided with at least 150mL live paramecia per day. From 14dpf to 20dpf, fish were fed with both live paramecia and dry food (Gemma 75). Beginning at 21dpf, fish were fed with dry food only. Larvae for experiments were obtained by crossing ATOH7-/- fish and following the breeding and collection protocol above.

TRPA1b KO and ATOH7 KO zebrafish analysis

To assess whether the novel hit compounds depend on the TRPA1b receptor to induce a phenotype, WT and TRPA1b KO zebrafish larvae were treated with the same compounds and the activity response compared. Due to limitations on the availability of KO fish, only five fish were used per well. Following selection of regions of interest (P1, full 1 minute stimulus, first

three 1 minute stimuli), the mean MI for each of these ROIs was calculated. Fold change vs. control was then determined by dividing by the equivalent MI values from background-matched DMSO controls. Significance between WT and TRPA1b KO responses was determined using Welch's t-test. To assess whether vision is required for the hit compounds to induce a phenotype, WT and ATOH7 KO fish were compared in a similar fashion. However, because the controls were too variable, mean MI values were used for comparison and to determine significance rather than fold change.

REFERENCES

1. Chen, J. & Hackos, D. H. TRPA1 as a drug target—promise and challenges. *Naunyn. Schmiedebergs. Arch. Pharmacol.* **388**, 451–463 (2015).
2. Paulsen, C. E., Armache, J.-P., Gao, Y., Cheng, Y. & Julius, D. Structure of the TRPA1 ion channel suggests regulatory mechanisms. *Nature* **525**, 552 (2015).
3. Cordero-Morales, J. F., Gracheva, E. O. & Julius, D. Cytoplasmic Ankyrin Repeats of Transient Receptor Potential A1 (TRPA1) Dictate Sensitivity to Thermal and Chemical Stimuli. *Biophysical Journal* vol. 102 23a (2012).
4. Bautista, D. M. *et al.* Pungent products from garlic activate the sensory ion channel TRPA1. *Proc. Natl. Acad. Sci. U. S. A.* **102**, 12248–12252 (2005).
5. Bessac, B. F. & Jordt, S.-E. Breathtaking TRP channels: TRPA1 and TRPV1 in airway chemosensation and reflex control. *Physiology* **23**, 360–370 (2008).
6. De Logu, F. *et al.* The acyl-glucuronide metabolite of ibuprofen has analgesic and anti-inflammatory effects via the TRPA1 channel. *Pharmacol. Res.* **142**, 127–139 (2019).
7. Viana, F. & Ferrer-Montiel, A. TRPA1 modulators in preclinical development. *Expert Opin. Ther. Pat.* **19**, 1787–1799 (2009).
8. Bautista, D. M. *et al.* TRPA1 mediates the inflammatory actions of environmental irritants and proalgesic agents. *Cell* **124**, 1269–1282 (2006).
9. Geppetti, P., Patacchini, R., Nassini, R. & Materazzi, S. Cough: The Emerging Role of the TRPA1 Channel. *Lung* **188 Suppl 1**, S63–8 (2010).
10. Nilius, B., Prenen, J. & Owsianik, G. Irritating channels: the case of TRPA1. *J. Physiol.* **589**, 1543–1549 (2011).
11. Kremeyer, B. *et al.* A gain-of-function mutation in TRPA1 causes familial episodic pain syndrome. *Neuron* **66**, 671–680 (2010).
12. Gracheva, E. O. *et al.* Molecular basis of infrared detection by snakes. *Nature* **464**, 1006–

1011 (2010).

13. Bellono, N. W., Kammel, L. G., Zimmerman, A. L. & Oancea, E. UV light phototransduction activates transient receptor potential A1 ion channels in human melanocytes. *Proc. Natl. Acad. Sci. U. S. A.* **110**, 2383–2388 (2013).
14. Birkholz, T. R. & Beane, W. S. The planarian TRPA1 homolog mediates extraocular behavioral responses to near-ultraviolet light. *J. Exp. Biol.* **220**, 2616–2625 (2017).
15. Du, E. J. *et al.* Nucleophile sensitivity of Drosophila TRPA1 underlies light-induced feeding deterrence. *Elife* **5**, (2016).
16. Guntur, A. R. *et al.* H2O2-Sensitive Isoforms of Drosophila melanogaster TRPA1 Act in Bitter-Sensing Gustatory Neurons to Promote Avoidance of UV During Egg-Laying. *Genetics* **205**, 749–759 (2017).
17. Zaidi, F. H. *et al.* Short-wavelength light sensitivity of circadian, pupillary, and visual awareness in humans lacking an outer retina. *Curr. Biol.* **17**, 2122–2128 (2007).
18. Harlan, G. C. Pupil Reflex in absolute blindness. *Trans. Am. Ophthalmol. Soc.* **7**, 671–677 (1896).
19. Fernandes, A. M. *et al.* Deep Brain Photoreceptors Control Light-Seeking Behavior in Zebrafish Larvae. *Curr. Biol.* **22**, 2042–2047 (2012).
20. Zoltowski, B. D. *et al.* Chemical and structural analysis of a photoactive vertebrate cryptochrome from pigeon. *Proc. Natl. Acad. Sci. U. S. A.* **116**, 19449–19457 (2019).
21. Shichida, Y. & Matsuyama, T. Evolution of opsins and phototransduction. *Philos. Trans. R. Soc. Lond. B Biol. Sci.* **364**, 2881–2895 (2009).
22. Cashmore, A. R. Cryptochromes: enabling plants and animals to determine circadian time. *Cell* **114**, 537–543 (2003).
23. Smith, L. Faculty of 1000 evaluation for A blue-light-activated adenylyl cyclase mediates photoavoidance in Euglena gracilis. *F1000 - Post-publication peer review of the biomedical literature* (2002) doi:10.3410/f.1005448.66255.

24. Montell, C. Gustatory receptors: not just for good taste. *Current biology: CB* vol. 23 R929–32 (2013).
25. Kokel, D. *et al.* Photochemical activation of TRPA1 channels in neurons and animals. *Nat. Chem. Biol.* **9**, 257–263 (2013).
26. Lam, P.-Y. *et al.* A high-conductance chemo-optogenetic system based on the vertebrate channel Trpa1b. *Sci. Rep.* **7**, 11839 (2017).
27. Echeverry-Gonzalez, C. A., Ortiz, A. & Insuasty, B. Rhodanine-based light-harvesting sensitizers: a rational comparison between 2-(1,1-dicyanomethylene)rhodanine and rhodanine-3-acetic acid. *New J. Chem.* **43**, 8781–8787 (2019).
28. McCarroll, M. N. *et al.* Zebrafish behavioural profiling identifies GABA and serotonin receptor ligands related to sedation and paradoxical excitation. *Nat. Commun.* **10**, 4078 (2019).
29. Nishimura, Y. *et al.* Pharmacological profiling of zebrafish behavior using chemical and genetic classification of sleep-wake modifiers. *Front. Pharmacol.* **6**, 257 (2015).
30. Rennekamp, A. J. *et al.* σ1 receptor ligands control a switch between passive and active threat responses. *Nat. Chem. Biol.* **12**, 552–558 (2016).
31. Jordi, J. *et al.* High-throughput screening for selective appetite modulators: A multibehavioral and translational drug discovery strategy. *Sci Adv* **4**, eaav1966 (2018).
32. Bruni, G. *et al.* Zebrafish behavioral profiling identifies multitarget antipsychotic-like compounds. *Nat. Chem. Biol.* **12**, 559–566 (2016).
33. Hill, K. & Schaefer, M. Ultraviolet light and photosensitising agents activate TRPA1 via generation of oxidative stress. *Cell Calcium* **45**, 155–164 (2009).
34. Kokel, D. *et al.* Rapid behavior-based identification of neuroactive small molecules in the zebrafish. *Nat. Chem. Biol.* **6**, 231–237 (2010).
35. Kay, J. N., Finger-Baier, K. C., Roeser, T., Staub, W. & Baier, H. Retinal ganglion cell genesis requires lakritz, a Zebrafish atonal Homolog. *Neuron* **30**, 725–736 (2001).

36. Ko, M. J. *et al.* A critical evaluation of TRPA1-mediated locomotor behavior in zebrafish as a screening tool for novel anti-nociceptive drug discovery. *Sci. Rep.* **9**, 2430 (2019).
37. Tesseromatis, C. & Alevizou, A. The role of the protein-binding on the mode of drug action as well the interactions with other drugs. *Eur. J. Drug Metab. Pharmacokinet.* **33**, 225–230 (2008).
38. Beers, M., Porter, R., Jones, T., Kaplan, J. & Berkwits, M. The Merck Manual. *Clinical Pharmacology & Therapeutics* **81**, 790–791 (2007).
39. Kheradpezhouh, E., Choy, J. M. C., Daria, V. R. & Arabzadeh, E. TRPA1 expression and its functional activation in rodent cortex. *Open Biol.* **7**, (2017).
40. Nau, R., Sörgel, F. & Eiffert, H. Penetration of drugs through the blood-cerebrospinal fluid/blood-brain barrier for treatment of central nervous system infections. *Clin. Microbiol. Rev.* **23**, 858–883 (2010).
41. Kokel, D. *et al.* Photochemical activation of TRPA1 channels in neurons and animals. *Nat. Chem. Biol.* **9**, 257 (2013).
42. Myers-Turnbull, D. *et al.* Simultaneous classification of neuroactive compounds in zebrafish. *bioRxiv* 2020.01.01.891432 (2020) doi:10.1101/2020.01.01.891432.
43. Lin King, J. V. *et al.* A Cell-Penetrating Scorpion Toxin Enables Mode-Specific Modulation of TRPA1 and Pain. *Cell* **178**, 1362–1374.e16 (2019).
44. WESTERFIELD & M. The Zebrafish Book : A Guide for the Laboratory Use of Zebrafish. *http://zfin.org/zf_info/zfbook/zfbk.html* (2000).
45. Burger, A. *et al.* Maximizing mutagenesis with solubilized CRISPR-Cas9 ribonucleoprotein complexes. *Development* **143**, 2025–2037 (2016).

Publishing Agreement

It is the policy of the University to encourage open access and broad distribution of all theses, dissertations, and manuscripts. The Graduate Division will facilitate the distribution of UCSF theses, dissertations, and manuscripts to the UCSF Library for open access and distribution. UCSF will make such theses, dissertations, and manuscripts accessible to the public and will take reasonable steps to preserve these works in perpetuity.

I hereby grant the non-exclusive, perpetual right to The Regents of the University of California to reproduce, publicly display, distribute, preserve, and publish copies of my thesis, dissertation, or manuscript in any form or media, now existing or later derived, including access online for teaching, research, and public service purposes.

DocuSigned by:

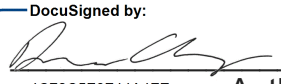

4C72C5F6F44A4FE...

Author Signature

6/3/2020

Date